GRADUATE SCHOOL OF PUBLIC HEALTH

UNIVERSITY OF PITTSBURGH

PITTSBURGH, PENNSYLVANIA 15213

GRANT NGR-30-011-096

MICROCHEMICAL SURFACE ANALYSIS BY ELECTRON SPECTROSCOPY

FINAL REPORT

July 26, 1971

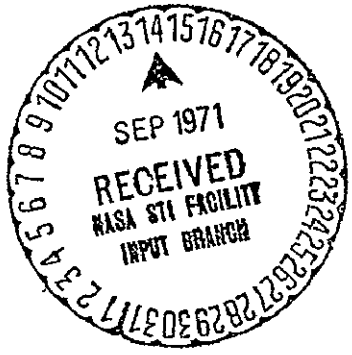

TABLE OF CONTENTS

1. INTRODUCTION

2. SUMMARY OF OBJECTIVES AND ACCOMPLISHMENTS

2.1 Auger Analysis

2.2 Characteristic Energy Losses

2.3 SEM Auger Detector Prototype

3. AUGER TECHNIQUES

3.1 Introduction

3.1.1 Recent Advances

3.1.2 Purpose

3.2 Theoretical

3.2.1 Secondary Electron Production and Characteristics

3.2.2 Auger Effect

3.3 Experimental

3.3.1 The Scanning Electron Microscope

3.3.2 Electronic Apparatus

3.3.3 Retarding Field Analyzer

3.3.4 127° Sector Analyzer

3.3.5 Cylindrical Mirror Analyzer

3.4 Summary

4. CHARACTERISTIC ENERGY LOSSES

4.1 Introduction

4.1.1 History

4.1.2 Interpretations

4.2 Theoretical

4.2.1 Review of Recent Literature

4.2.2 Correlation between Characteristic Energy Losses and Ionizational Potential

4.3 Experimental Techniques

4.3.1 Cylindrical Mirror Analyzer

4.3.2 Detection and Recording of Spectrum

4.3.3 Measured Characteristic Energy Losses in Aluminum

4.4 Conclusion

5. SEM AUGER DETECTOR PROTOTYPE

5.1 Instructions

5.2 Circuit Diagrams

5.3 Detector Drawings

5.4 Parts List

6. TABLES AND FIGURES

7. REFERENCES

"Microchemical Surface Analysis by Electron Spectroscopy"

Final Technical Report

Grant No. NGR 39-011-096

1. Introduction

This final report is the result of a one year research and engineering effort. It has been divided into four main parts: Section 2 restates the original objectives and briefly summarizes the work carried out. Sections 3 and 4 provide a discussion of the technical results and Section 5 contains the detailed instructions and all the necessary drawings for the operation of a prototype Auger analysis system delivered to the N.A.S.A. Langley Laboratories. The final part,Section 6,contains an outline of the most significant accomplishments under this grant and discusses the areas of future work necessary to take full advantage of these accomplishments.

2. Summary of Objectives and Accomplishments

The program undertaken had basically two aims:

2.1 To develop an Auger electron velocity analyzer suitable for the specific requirements of the SEM, a prototype of which will be delivered to the NASA Langley Laboratory for use in their study of surface phenomena on semi-conductor devices.

2.2 To carry out fundamental studies on Auger and Characteristic electron energy loss peaks in an effort to elucidate the various physical mechanisms responsible for the different types of characteristic-losses and the factors determining the shapes and position of Auger and Characteristic peaks in order to permit eventual quantitative analysis by electron spectroscopy.

2.3 With regard to the development of an Auger analyzer for use in an SEM, the initial effort was directed towards the design, construction and testing of a new type of opposing-potential device of large acceptance angle and high sensitivity, using a scintillator and photomultiplier as detector. A prototype was successfully operated and demonstrated the following important points:

a. Auger analysis is possible with beam currents at least as small as 10^{-8} amp, possibly considerably smaller after optimization of detectors and amplifier circuits.

b. Contamination rates can be sufficiently low in an ion-pumped, unbaked vacuum system to make Auger analysis a practical technique in conjunction with scanning electron microscopy. However, special vacuum modification will most likely have to be made in order to obtain low rates of contamination on a routine basis.

c. Resolution of electron peaks is more than adequate to meet the needs of Auger spectroscopy and can easily be varied by changing the position of the analyzer, thus permitting a choice of either high resolution at lower collection efficiency or lower resolution at increased collection efficiency.

d. The analyzer configuration is such that it can be used also to generate a picture signal representing either a total secondary electron and backscattered electron picture or only a backscattered electron image.

A cylindrical type of velocity analyzer was also designed and built. This type of analyzer has a distinct advantage over other types

of analyzers in that it has a larger collection efficiency since the acceptance angle revolves azimuthally around the axis of symmetry. It is also a narrow band filter, thus preventing high energy electrons from reaching the electron detector that add to the noise, resulting in a higher signal to noise ratio. However, since this analyzer requires a more precise positioning of the specimen and electron beam, it may prove to have some disadvantages in ease of operation of the scanning microscope compared with the less critical opposing potential analyzer.

With regard to the fundamental study of Auger and characteristic loss peaks, equipment was designed, constructed and assembled to carry out a fast coincidence type of experiment to determine which of the characteristic losses experienced by an individual electron are most strongly associated in time with the ejection of a secondary electron. However, due to the lack of time, no coincidence experiments were made. Instead, most of this study was carried out in the reflected mode from a thick sample such as is commonly studied in the SEM. Using the cylindrical analyzer, characteristic energy losses were measured in Al, Cu and Au samples.

A study correlating the known characteristic losses of the elements with their ionization potential and position in the atomic table provided strong evidence that the majority of these losses are probably of the direct ionziation or individual collision type, connected with the ejection of a secondary electron.

3. Auger Techniques

3.1 Introduction

The possibility of identifying low concentrations of elements on surfaces by analyzing the velocity of Auger electrons ejected under electron bombardment was pointed out by Lander[1] and reduced to a practical technique by Hafner[2], Weber[3], and others through the use of ac amplification.

Recent experimental work has demonstrated that very small concentrations of chemical elements can be detected on or near surfaces in typical concentrations as low as 10-20 ppm. One fiftieth atomic layer of cesium on gold has been detected, and some 10 ppm of sulfur has been measured on nickel surfaces. Low atomic number elements such as lithium, beryllium, boron, carbon, nitroge n, oxygen, and phosphorus are readily resolved, since their Auger peaks are typically spaced 60-110 eV apart a large spacing compared to the resolving power of all velocity analyzers.

This technique has been successfully applied to the detection of small traces of organic solvents of residues of phosphorous from plating processes, and of segregation of maganese on steel specimens in the identification of surface and grain-boundary segregation.

Although a rough proportionality between weight concentration and intensity of the Auger lines has already been demonstrated, the reproducibility is not yet sufficient for precise quantitative analysis. Work is currently proceeding in a number of laboratories to achieve better reproducibility and to improve signal to noise ratios, so that the present qualitative analysis capability should be supplemented by a quantitative capability comparable to that of x-ray analysis today.

Since the Auger electrons have a relatively short range in matter they are strongly sensitive to even small amounts of surface contamination. For this reason only a system equipped with ion-pumping, in which no organic oils are present to deposit carbon films under electron bombardment, is currently capable of utilizing the Auger analysis technique. Not only do ion-pumped systems permit the attainment of total pressures as low as 10^{-8} torr but they allow very much lower partial pressures of organic vapors to be obtained so that the rate of build up of surface contamination can be considerably reduced.

Briefly, the Auger effect may be explained as follows: When an electron in the K shell (the innermost shell) of an atom is ejected, another electron from one of the outer shells of the same atom may fall to the K shell and take up the vacancy, with the consequent emission of a K x-ray photon. Occasionally, this K x-ray photon is not observed, but its energy is used to eject a second electron from one of the upper shells of the same atom, leaving this atom doubly ionized. This phenomenon was first observed by Auger in 1925. Subsequently, it was known as the Auger effect, and that second ejected electron as the Auger electron.

Although Auger electrons were first produced by x-rays ionizing the inner atomic shell, Lander[4] and subsequent investigators employed an electron beam to unlock the Auger electrons for analytical purposes. Such a beam from a scanning electron microscope can be readily focused and deflected and can produce a much larger Auger current from a small sample than can x-ray excitation.

Since the primary electron beam current is very low--in the order of nano-ampere or lower in a scanning electron microscope--Auger

spectroscopy is also non-destructive. With its high resolution, contrast and magnification, the scanning electron microscope is also an ideal probing tool for other surface studies. Auger electrons ejected from very small concentrations of foreign atoms in a sample (in the order of tens of ppm) make it possible to detect minute quantities of trace elements and their distribution in various materials. The excellent resolution in a scanning electron microscope also enables it to localize the trace elements to within one or two hundred Angstroms. Finally, the ability of the primary electron beam to scan over a very small area puts the Auger techniques by scanning electron microscopy in a unique position not surpassed by any other at the present state of the art.

3.1.1 Recent Advances in Auger Work

Many improvements have been made in this field since Lander's pioneering work in 1953. Tharp and Scheibner[5] have shown that Auger peaks could be detected using a three grid LEED (Low Energy Electron Diffraction) system as a retarding field analyzer. They obtained the energy spectrum by electrical differentiation of the retarding field plot in which a small AC modulating voltage is applied to the retarding grid and the collector is tuned to the frequency of the applied signal. Harris[6] showed that the Auger spectrum sensitivity is enhanced by electronic differentiation of the energy distribution function by using a 127° sector electrostatic deflection analyzer. Bishop and Reviere[7] have evaluated the efficiency of Auger electron production and concluded that for low Z elements, one should get about two Auger electrons for each 10^5 primary electrons or about 20 pA for 1μA of primary beam at a 17% collection efficiency. Since each element intercepted can be registered it is possible to use incident

beam currents of 10^{-10}-10^{-9} A and still get acceptable output rates of a few thousand Auger electrons per second. Recent work by McDonald and Palmberg[8] at North American-Rockwell Science Center using an ultra-clean ion-pumped SEM clearly shows that qualitative elemental analysis with distinct, reproducible Auger peaks is possible with beam currents of about 1nA.

3.1.2 Purpose

Presently, several laboratories are actively working on Auger spectroscopy. However, many questions have not been answered satisfactorily. It is not clear to what extent the resolution, sensitivity and signal to noise ratio are affected and limited by different parameters such as the primary current, voltage, geometry of the primary beam with respect to the sample, the modulating AC signal, and so forth. The purpose of this work is therefore to explore in a SEM environment:

(1) The possible resolution of each of the three basic tehcniques--the retarding field, the 127° electrostatic sector and the 180° cylindrical mirror detector system.

(2) The limits due to other considerations. and

(3) Comparison of the relative performance of each system from a S/N point of view.

3.2 Theoretical

3.2.1 Secondary Electron Production and Characteristics

Research in low energy electron spectroscopy requires the understanding of secondary electrons and so a discussion is in order. A primary electron beam strikes a clean specimen, and causes emissions of electrons consisting of three general categories: high energy backscatter primary

electrons, low energy secondary electrons, and an intermediate energy range of scattered or rediffused primary electrons plus secondary electrons (Fig. 1).

An important feature of secondary electrons is the energy dependency of the secondary yield δ, the ratio of number of emitted to incident primary electrons, a value which rarely exceeds two. Another parameter is the backscattered coefficient η, the ratio of number of backscattered to primary electrons; its value may be as high as 0.5 for some high Z elements. These two types of electrons are characterized by their energy distribution. The true secondaries are characterized by their low energy peak at about 2 ev for most metals and follow a quasi-Maxwellian energy distribution with a mean value of 5 or 6 ev, independent of the primary energy. Backscattered electrons emerge with energies above 50 ev and increase all the way up to the primary energy. Only a small percent are truly elastically reflected, i.e., with little or no energy loss in the specimen.

η varies linearly with Z and remains almost constant with changing primary energy for elements with $Z \leq 30$. And for higher Z elements, η increases slowly with primary energy.

Oxides or surface contaminants will increase the secondary yield considerably because elastic collisions become dominant and the secondaries' mean free path is larger here than in metals. Most any amount of energy can be absorbed by the valence and conduction electrons in a metal; the secondaries have a shorter mean free path, and the yield is therefore lower. The yield values for many metals and oxides have been tabulated in Reference 17.

The theory of secondary emission was first approximated by the Whiddington law.[9] In light of current theory, which turns out to be more compatible with experimental data, the Whiddington law is not strictly applicable for low energy electron bombardments because (1) the primaries do not travel in a straight line, and (2) inelastic scattering becomes more important at low energy. An up-to-date account for the secondary process is summarized as follows. On entering the surface, the primaries undergo rapid inelastic scattering with the loosely bound electrons in the outer shells as well as with the more firmly bound electrons in the inner shell, resulting in the production of fast secondaries, x-rays and Auger electrons. The mean energy loss of these primary collisions is in the order of 70 ev for all substances, but the mean energy expended per secondary is in the order of 20-35 ev. As a result of the rapid primary scattering, the primary electrons loose their initial direction quickly and diffuse at random beginning at a depth equal to the scattering mean free path for the primary electron. Ionization density reaches a maximum at this depth, which may also be regarded as the zone of origin of most of the secondaries. The theoretical description therefore involves (1) writing an expression for the ionization as a function of depth, and (2) calculating the probability that the secondaries formed will reach and escape the surface.

The secondaries formed in the sample have equal probability to migrate in all directions. On their way to the surface, the secondaries are able to excite and ionize the atoms close to their path since the electrons all possess an energy of about 0-30 ev (the mean energy about 5 to 6 ev). In metals and semiconductors where the energy gap is small,

the probability for inelastic collision is large, resulting in very short secondary mean free paths. The escape probability may be assumed to obey an exponential law. The shape of the yield curve is a result of two opposing effects: (1) an increase in the total number of secondaries formed with increased primary energy, and (2) the reduced probability of reaching the surface as the primary energy is increased and the depth of formation grows in approximate proportion to the primary electron mean free path for large-angle scattering.

The electrons in the broad range between 50 volts and the high energy end of the backscattered electron spectrum are especially important for sample analysis. The velocity distribution of these electrons is related to the atomic shell structure of the elements in the few top layers of material in or at the sample surface. This is the basis for the Auger analysis.

3.3.3 The Auger Effect

A detailed quantum mechanical treatment of the Auger process is given in Reference 19. The Auger effect was discovered in the course of x-ray fluorescence yield study.

When a substance, which for simplicity is assumed to contain only one kind of atom, is irradiated with a beam of x-rays or electrons, K photo-electrons will be assumed to be ejected from n_K atoms per second. In the steady state, the same rate of atoms are also returning to the non-ionized or normal configuration. Of these n_K atoms, a number n_1 will emit the $K\alpha_1$ line as a step in the process, n_2 will emit $K\alpha_2$, and so on. The fluorescence yield for the K level, w_K, is defined as

$$w_K = \frac{n_1 + n_2 + n_3 \cdots}{n_K} = \frac{\Sigma\, n_f}{n_K} \qquad (1)$$

At first thought it would seem that the fraction w_K must be unity, since in order to replace the vacancy in the K shell, an electron must drop in from the L, M,N,...shell with the concomitant emission of a quantum of K series radiation. The earliest experiments indicated that w_K is distinctly less than one. Kossel[10] remarked that the fractional value of w_K might be due to a radiationless transfer of energy to an electron, the transfer taking place within the parent atom. This type of transfer may also occur in a gas when an excited atom transfers its energy to another atom on impact. Such internal conversions are known to occur in radioactive processes since beta-rays appear whose kinetic energies are given by the energy of a nuclear gamma-ray minus the binding energy of the K or L shell. Such an effect in the x-ray region would tend to decrease the yield of fluorescence radiation and increase the yield of beta-rays from the ionized material. The existence of internal radiationless transfer in the x-ray region was first clearly shown in Wilson cloud chamber tracks by Auger, who gave the following explanation.

When a K photo-electron is ejected from an atom, the vacancy in the K shell may be filled by one of the L electrons, but it is not necessary that one quantum of K radiation actually leave the atom. Instead, the quantum of K radiation may be absorbed or converted by the L shell, for instance, into the energy necessary for the ejection of an L' electron plus the kinetic energy of the beta-ray produced. Thus if $(1/2)\ mv^2$ is the kinetic energy of the Auger electron (neglecting relativistic effect)

$$(1/2)\ mv^2 = h\nu_\alpha - (E_L^{II} - E_L) \qquad (2)$$

where E_L^{II} is the energy of an atom with two L electrons missing, and

the energy difference in parentheses is the work required to remove the second L electron. But

$$h\nu_{\alpha} = E_K - E_L \qquad (3)$$

Hence

$$1/2mv^2 = E_K - K_L^{II} \simeq E_K - 2E_L \qquad (4)$$

by making the assumption that the energy required to remove the second L electron is the same as required to remove the first. It is also possible that the quantum having the wavelength of the Kα line may eject an electron from the M levels, leaving the L undisturbed. In this case the kinetic energy of the Auger electron would be

$$1/2mv^2 = h\nu_{\alpha} - (E_{LM} - E_L) = E_K - E_{LM} \qquad (5)$$

where E_{LM} denotes that state with an L and M electron missing, i.e. with an energy $(E_L + E_M)$. If this process is repeated a step further, it may be that the two vacancies produced in the L shell will be filled by the transfer of two M electrons, and that the quanta thus liberated be absorbed in the M shell, producing two more Auger electrons from the same atom. These may be called secondary Auger electrons. Their energies will be less than that of the primary Auger electron. Auger observed such secondary electrons from Br-35 and higher atomic number gases. In these heavier gases, point or sphere tracks were also occasionally observed, and were attributed to the tertiary Auger electrons ejected from the N shells by radiation resulting from the filling of vacancies in the M shells. In heavier elements Auger was also able to estimate the L-level fluorescence yield. His results are given in Table 1. Subsequently various investigators measured fluorescence yields

in the K and L levels of many elements, and their results are summarized in Table 2 and Fig. 2. The difference between the fluorescence yield and unity is the Auger electron yield. Finally it was shown that the probability of fluorescence yield is given by

$$w = (1 + aZ^{-4})^{-1} \qquad (6)$$

where $a = 1.12 \times 10^{6}$ for K electrons, or
$a = 6.4 \times 10^{7}$ for L electrons

and Z = atomic number

Most Auger spectroscopic work involves a maximum primary energy of about 2 kev. This implies an Auger electron arising from a K-shell ionization cannot be observed above $Z = 14$ (Si), from L-shell ionization above $Z = 36$ (Kr), and from M-shell ionization above $Z = 65$ (Tb). Thus eq. (6) shows the maximum values of w corresponding to that Z for which K and L-shell ionizations are possible are 0.033 and 0.026 respectively. Below a primary energy of 2 kev, the probability of photon production is negligible; that is, most ionization will produce Auger electrons.

3.3 Experimental

3.3.1 The Scanning Electron Microscope

The scanning electron microscope was developed over the past several decades as a means to examine in detail objects that could not be so examined previously. The optical microscope, limited by the wavelength of light and index of refraction of lenses, cannot resolve less than 2000 Å, and for practical purposes its usefulness ends at 2000x magnification. The conventional transmission electron microscope is able to attain a resolution of 5 Å and a magnification of several hundred thousand times. However it is limited by very low contrast and thin specimens, which may be destroyed in the course of examinations.

The scanning electron microscope bridges the gap between these two devices but obviates their defects. Its resolution is better than 200 Å, and magnification 100,000x. Yet it has a depth of field of up to 500 times that of the other instruments. The scanning microscope can operate at power levels not destructive to the specimen, and requires little preparation other than mounting. It is possible to do one or more modes of operation simultaneously, such as the examination of backscattered, transmitted, secondary and Auger electrons, induced and absorbed current. Installation of a Si(Li) detector permits x-ray analysis to be carried out. Therefore the SEM combines the precision and versatility of an analytical instrument with the ability to visualize structures down to a few hundred Angstroms in size.

The scanning electron microscope examines the physical topography of a wide variety of specimens by presenting a magnified secondary electron emission image of the specimen on a cathode ray tube. As a microscope, the SEM "sees" with a very fine beam of electrons sharply focused with magnetic lenses onto the specimen surface in a spot as small as 0.01 micron. Magnetic deflection coils move this spot across the surface of the specimen in a scanning sequence similar to that used in television. As the primary electrons strike the specimen they cause the specimen to emit lower energy electrons in quantities determined by the primary beam voltage, nature of the specimen and the beam incidence angle. A portion of these emitted electrons is collected and detected. The current output is converted to a voltage, amplified, and used to control the brightness of a display cathode ray tube whose electron beam is moved in synchronism with the primary beam on the specimen. The cathode ray tube thus presents an image of the specimen surface.

The three-element type electron gun uses an adjustable heated hairpin tungsten filament as a cathode. The emitted electrons are accelerated by an applied voltage variable from 1 to 30 KV. Two condensing lenses and a final objective lens focus the primary beam to a spot of less than 0.01 micron in diameter at the specimen. All three lenses are pre-aligned, and each is fitted with a set of aperatures adjustable under vacuum. An eight pole electrostatic stigmator is provided in the objective lens. Phosphor beam finders and a microscope permit precise alignment of the beam.

Resolution at the sample is a function of the primary beam voltage, the focused spot diameter and the specimen. At 20 KV the resolution is at least 200 Å and can be better than 100 Å under optimum conditions.

Magnification is the ratio of the line length scanned on the display tube to that scanned on the specimen. Focus remains constant and does not affect magnification. The raster can be reduced from more than 5 mm to less than 5 microns line length, permitting a magnification range from 10 to 100,000x.

3.3.2 Electronics for the Detection of Auger Electrons

Electrons after surmounting the retarding barrier or surviving the narrow slits of the electrostatic analyzers, will be accelerated by a 10 KV potential to strike a plastic scintillator. The light generated is transmitted by a solid glass light pipe to a photomultiplier located outside the vacuum chamber. The photomultiplier output may be fed either to video amplifiers and displayed on the cathode ray tube, or to the electronic system for Auger analysis. It should be pointed out here that output signals from both the retarding field and cylindrical analyzers can be used to generate visual images on the CRT.

The plastic scintillator and photomultiplier assembly can be replaced by a simpler electron detector---the Bendix Spiralton. This device employs a continuous semi-conducting dynode surface with high gain and low noise characteristics. Furthermore, its operation requires a substantially lower power supply voltage, and the effect of strong electric fields may be obviated.

The electronics also include the sweep chassis, the lock-in amplifier and the XY recorder which displays the results. The sweep chassis contains an audio oscillator to modulate the sweep voltage applied to the retarding grids or deflectors in the analyzer, and the ramp function sweep voltage power supply.

The lock-in amplifier (PAR-HR8) is used to measure the amplitude of the signal recovered in the scintillator collector. Since this signal is present in a high noise background, special means must be used to extract this signal, hence the use of this amplifier. Its basic element is a phase sensitive detector in which the signal to be measured is mixed with a reference signal of the same frequency, thus producing sum and difference frequencies. Here the reference is the signal derived from the audio oscillator used to modulate the retarding grid or deflector sweep voltage supply. A low-pass filter at the output of the mixer rejects the high frequency components corresponding to the sum frequencies and passes the difference frequencies which lie within its pass band. By making the bandwidth of the filter narrow, the effect of input noise is reduced, resulting in a greatly improved signal to noise ratio.

3.3.3 The Retarding Field Analyzer

Geometrically, the retarding field analyzer used in the SEM as shown in Fig. 3 is a smaller version of a standard LEED analyzer which has been demonstrated by Tharp and Scheibner,[11] and Weber and Peria[12] in their three-grid LEED systems. However, the main difference between these two analyzers lies in their electron detectors. The retarding analyzer uses a more efficient scintillator which has been described earlier. It has been estimated that for every electron incident onto the scintillator, at least 2.2 electrons are produced at the photocathode. On the other hand, LEED system employs a fluorescent screen (with no multiplication) as the electron detector. This technique is less efficient resulting in an inferior signal-to-noise ratio. More recently, Plamberg and Taylor[13] demonstrated higher resolution in a four-grid LEED system, a schematic diagram of which is shown in Fig. 4. The retarding field voltage is applied to the middle grid along with a small AC modulating signal, and the retarding voltage and amplifier output are fed to the X and Y channels of a recorder. When measuring the derivative of the energy distribution, the signal channel of the lock-in amplifier is tuned to a frequency double that applied to the retarding field grid, and this double frequency is also applied to the reference channel of the lock-in amplifier. This method permits significant noise suppression because the effective band width of the synchronous detector can be made very small. The signal gain can be increased because the slowly varying portions of the energy distribution curve contributes little to the derivative. The resulting curve is shown in Fig. 5.

The mathematics derived for a LEED system may be applied to a retarding field analyzer, and only the results and assumptions will be

quoted here. Consider the collected current I(V) (See Fig. 4) as a function of the scanning voltage V. If a small AC signal k sin ωt is applied to the retarding grid, then a Taylor series expansion of I(V + k sin ωt) may be carried out. The amplitude of the fundamental (proportional to the slope of the retarding field plot) A_1 is found by keeping just the first term of the Taylor expansion

$$A_1 = k\, I'(V) \qquad (7)$$

and the second harmonic (proportional to derivative of energy distribution) A_2 is similarly

$$A_2 = (k^2/4)\, I''(V) \qquad (8)$$

provided k is sufficiently small. Furthermore it is assumed that each Auger peak is in the shape of a Gaussian distribution containing a total current i such that

$$I'(V) = i\, (1/\delta\, (2\pi)^{1/2}) \exp\, (-Vx^2/2\, \alpha^2) \qquad (9)$$

where 2σ is the full width at half maximum of the Gaussian Auger peak.

In order that eqs (7) and (8) hold true with an error of 5% or less, k must be restricted to be less than $(1/2)\sigma$. Typically, σ is 5 to 10 volt wide. From eq (9), it can readily be shown that

$$A_1\ (\max) = 0.4\ (k/\sigma\ )i \qquad (10)$$

and

$$A_2\ (\max) = 0.006\ (k/\sigma\ )^2 i \qquad (11)$$

These results have also been independently arrived at by Bishop and Riviere.[14] As it will be shown later, eqs (10) and (11) are necessary for the evaluation of the signal-to-noise ratio.

When a monoenergetic electron beam of energy E is measured by any detector, the output signal will not appear as a sharp line. Instead,

it will exhibit a shape approximated by a Gaussian curve whose full width at half maximum (FWHM), or ΔE, will be a measure of the instrumental limitations. Resolution is defined as the ratio of $(E/\Delta E)$, or as the instrumental line width (ILW), its reciprocal. When the percent of error is proportional to the electron energy E, then the ILW is a constant. For example, the plane of the retarding wires in a standard 3-grid system is not an equipotential surface. That is, a small potential difference ΔV lies across the center of the grid aperture and the grid wires. A typical $\Delta V/V$ value is about 2%. Improvements can be made by using the finest mesh grid and/or decreasing the grid spacing, at the expense of additional unwanted secondary electrons created at the grid. A more practical solution has been the replacement by a double retarding grid.

If θ is the angle of divergence of the incoming electron with energy $E=ev$, then the potential required to cut off these electrons will be ΔV less than that for those electrons coming in at normal incidence. It has been shown that

$$\frac{\Delta V}{V} = \frac{\Delta E}{E} = 1 - \cos^2\theta = \sin^2\theta \qquad (12)$$

ΔE then represents the limiting resolution of the retarding geometry, and in principle, can be reduced to any desired limit by aperturing the beam in angle. Ideally, the retarding grid should be spherical so that electrons go through the mesh at normal incidence. A plane grid undoubtedly will cause the cutoff to occur at reduced retarding potential, thus degrading the resolution. However, this factor is not important with a small aperture such as that shown in Fig. 3.

Mis-positioning of the sample will cause the electrons to enter the retarding field in an off-normal fashion. The resolution will only be

slightly impaired by the $\sin^2\theta$ term in eq (12). A plot of the theoretical line width for an opening angle is shown in Fig. 6 and 7. Typically, the opening aperture radius is 0.5 cm and 5 cm away from the sample. The sine of the half angle is 0.1, and the resolution, which is proportional to $\sin^2\theta$, is 1%. Improvement in resolutions may be made by either reducing the aperture or increasing the sample aperture distance. As an example, some preliminary data shows when the detector opening is several mm from a gold sample, the 55, 60 and 80 ev peaks are broad and cannot be resolved. When the sample aperture distance is increased by about 2 cm (corresponding to $\Delta E/E = 7\%$), the peaks are resolved (Fig. 8), and the $\Delta E/E$ value is approximately 16%.

Variation of the work function over the retarding grid surface will give rise to a certain energy spread ΔE. Its exact value is exceedingly difficult to evaluate because it is easily modified by surface contaminants. This ΔE value is estimated to be in the order of 0.1 ev , and so it is not very important in Auger type qualitative analysis.

Modest magnetic shielding will reduce ΔE to less than 0.1 ev. Stray DC magnetic fields become important for $(\Delta V/V) = .25\%$ at energy under 20 ev.

Another effect is the AC modulation of the retarding grid, whose peak to peak amplitude will be at least equal to the energy width of the Auger electron as discussed earlier.

Sensitivity is the ability of a detector to measure a signal in the presence of background noise. This depends on (1) the gain of the detector, (2) the noise of the detector and (3) the amount of noise accompanying the signal. In the analyzers to be discussed, the gain is unity.

There are several sources of noise. A first one is the flicker effect noise associated with the transistor amplifier circuits. This noise spectrum varies roughly as 1/f, and so it can be minimized by operating above 1 KHz. It has been shown that this noise is insignificant compared with the shot noise. The PAR-HR-8 manual describes the variation of this noise level as a function of the modulating frequency and amplifying circuit resistance. For a 1m ohm resistance, the optimal frequency may range from several hundred to several thousand Hz/per second. Harris and Taylor[15] tuned their detectors to 7 KHz and 0.4 KHz, respectively. It appears one must search an optimal frequency for his system by trial and error within the above range.

Secondly, there is a thermal or Johnson noise in the input resistor to the lock-in amplifiers. The rms voltage is given by:

$$Vrms = (4\ R\ kTB)^{1/2} \qquad (13)$$

where R is the resistance in ohms, k the Boltzman's constant, T the absolute temperature, and B the bandwidth in cps. For example, some typical values at room temperature are R = 1 M ohm, B = 0.125 cps (corresponding to a time constant of 1 sec), kt = .025 ev, then

$$Vrms = 0.045 \text{ micro volt}$$

By far the most important is the shot noise, which is given by:

$$Vrms = (2\ e\ I_o\ R^2\ B)^{1/2} \qquad (14)$$

where e is the charge of an electron, I_o is the current leaving the sample and being collected, and R and B are defined above. If I_o = 10 microamp such as in a LEED system, then Vrms = 0.63 microvolt, which is an order of magnitude higher than the thermal noise. If I_o = 0.1 microamp, the upper limit in the SEM, then Vrms = 0.063 microvolt. However, the most important consideration is the signal-to-noise ratio at the detector input.

Previous discussions have assumed that an Auger peak has the shape of a Gaussian distribution. If i is the current under this peak, then i is given by:

$$I = s\, T_R\, I_P \qquad (15)$$

where s is the ratio between the total Auger current under the peak of consideration and the primary beam current I_p (a typical value of s is 10^{-4}); and T_R is the fraction of this Auger current passing through and reaching the scintillator. Then the maximum rms signal across the sensing resistor at the 1st harmonic will be:

$$V_1 = (2)^{-1/2} 0.4(\kappa/\sigma)\, i\, R = .28(\kappa/\sigma) s\, T_R\, I_P\, R \qquad (16)$$

and the 2nd harmonic will be

$$V_2 = (2)^{-1/2} .06(\kappa/\sigma)^2\, i\, R = .042(\kappa/\sigma)^2 s\, T_R\, I_P\, R \qquad (17)$$

In order to determine the shot noise, it is convenient to assume the secondary electron energy spectrum to be uniformly distributed so that the total current under this rectangular distribution is ηI_p where η is a back scatter coefficient. This assumption will be grossly erroneous at both extreme ends of the spectrum, where, fortunately, it is the area of least interest. If an Auger peak is to be examined at some V_A, by means of a retarding potential analyzer then only those electrons whose energy is higher than V_A are responsible for the shot noise in the detector. The current reaching the detector is

$$I_p\, T_R (V_P - V_A)/V_p = I \qquad (18)$$

where V_p is the maximum primary voltage, and I_o has been defined in eq (14).

The signal-to-noise ratio of the fundamental and secondary harmonic frequencies are respectively,

$$\frac{V_1}{V_n} = \frac{.28(\kappa/\sigma)s\ T_R\ I_p\ R}{5.6 \times 10^{-4}\ (I_p\ b\ B)^{1/2}} = 5 \times 10^8\ (\kappa/\sigma)\ \frac{(s^2 T_R{}^2 I_p)}{bB} \qquad (19)$$

$$\text{and } \frac{V_2}{V_n} = 7.5 \times 10^7\ (\kappa/\sigma)^2\ \frac{(s^2\ T_R{}^2\ I_p)^{1/2}}{bB} \qquad (20)$$

where typically $R = 10^6$ ohm

$$\text{and } b = \pi T_R\ \frac{(V_p - V_A)}{V_p} \qquad (21)$$

3.3.4 The 127° Sector Analzyer

An alternate to the retarding field analyzer is the 127° electrostatic sector velocity analyzer by Hughes and Rojansky.[16] If V_D is the potential across the deflecting plates of radii R_1 and R_2, then electrons with energy eV_A will emerge from the exit slit under the condition

$$(1/2)V_D = V_A\ \ln\ (R_2/R_1) \qquad (22)$$

If W is the slit width and Ro the mean radius of the plates, and if the electrons enter with a uniform energy distribution, then $(\Delta V/V)$ is given by

$$\Delta V/V_A = W/Ro \qquad (23)$$

A schematic diagram of the 127° sector such as used by Harris[17] is shown in Fig. 9. In his case, the electron gun produces a current of several hundred microampere in a 2 mm wide beam, striking the sample at about 15° incident angle. In the SEM, both the primary current and beam diameter are greatly reduced (e.g. 0.1μ amp and 1 micron wide). The effective current is also smaller because the analyzer accepts electrons only from the portion of the sample very near its optical axis. A typical mean radius of the analyzer is 2.5 in. and the slit width of 0.005 in., and a resolution of about 0.2% could be expected. Under optimal conditions

an energy difference of less than 3 eV in 1000 eV could be resolved. Electrons leaving the analyzer enter a shielded secondary emission Bendix multiplier. Electron energy distributions are observed by slowly sweeping the analyzer deflection voltage through its range. Most observations are made, however, not on the energy distribution itself but on its derivation with respect to energy. A small AC perturbation is applied to the swept analyzer deflection-plate potentials, and the corresponding AC component in the multiplier output is amplified and measured synhronously with the phase sensitive detector.

If the sector is adjusted only to accept electrons with energy eV_A, then the current reaching the analyzer will be $dI/dV\big|_{V_A \Delta V}$. By following the same procedure as in the retarding field section, one may expand a Taylor series of $(dI/dV)(V + k \sin wt)$, and the first harmonic may be shown to be:

$$B_1 = k\, L''(V) \qquad (24)$$

provided k is sufficiently small. At the maximum of B_1, $Vx = \sigma$ (assume again that the current i follows a Gaussian shape), and $I''(V) = 0.242\, i/\sigma^2$ For $(k/\sigma) = 0.5$, a 6% error is introduced by neglecting higher order terms in the Taylor expansion.

In the case of the retarding analyzer, shot noise, the dominant noise, arises from all the current reaching the detector. However, in the 127° analyzer, the direct current reaching the electron collector has a very narrow energy band corresponding to V. This is the main advantage of the sector analyzer. This current i:

$$i = s \cdot I_p\, T_s \qquad (25)$$

where T_s is the transmission efficiency of the sector; T_s is analogous to T_R in the case of the retarding analyzer. Then the signal-to-noise ratio is found to be (from eqs 24, 25, 14)

$$\frac{V_s}{V_n} = \frac{.242\ (2)^{-1/2}(\kappa/\sigma^2)\ i\ R\ \Delta V}{5.6 \times 10^{-4}\ (I_o\ B)^{1/2}}$$

$$= 3.05 \times 10^8\ (K/\sigma)(\Delta V/\sigma)\ \frac{(s^2\ I_p\ Ts}{\eta\ B}\ \frac{V_A}{\Delta V})^{1/2} \qquad (26)$$

3.3.5 The Cylindrical Mirror Analyzer

The most promising technique, however, appears to be the cylindrical mirror analyzer first studied by Blauth,[18] then later by Zashkvara.[19] Recently the dynamic and electro-optical properties of this analyzer were examined in detail by Sar-el and Hafner.[20] Fig. 10 shows a schematic diagram of the analyzer whose deflection equation is governed by

$$E\ /eV = 1.3/\ln\ (r_2/r_1) \qquad (27)$$

where V is the potential difference between the two concentric cylinders with radii r_1 and r_2, and Eo is the kinetic energy of the electron emitted by a point course S on the axis. Refocusing occurs at $L_o = 6.1\ r_1$, $\alpha_o = 42.3°$ and the maximum distance off axis is $r_m = 1.8\ r_1$.

This analyzer has distinct advantages over the previous two in that it has a larger collection efficiency since the acceptance angle revolves azimuthally around the axis of symmetry, and it still rejects a wide noise band. The feasibility of this detector has been demonstrated recently by Palmberg.[21] However, the response is also more position sensitive, and it is imperative that the electrons enter the capacitor at 42.3°.

The mathematics for carrying out the signal and noise calculations in the case of the cylindrical analyzer is essentially the same as that

for the 127° electrostatic analyzer. Following the same argument presented in the previous section, one finds the 1st harmonic signal-to-noise ratio to be

$$\frac{V_s}{V_n} = 3.06 \times 10^8 \, (k/\sigma) \, (\Delta V/\sigma) \, \frac{s^2 \, I_p \, T_c}{\eta B} \, \frac{V_A}{\Delta V} \qquad (28)$$

where Tc is the transmission coefficient for the analyzer.

3.4 Summary

The performance of three different Auger analyzers has been discussed. An interesting and useful evaluation would be the comparison of their relative signal-to-noise ratio. First the results may be summarized as follows:

Analyzer	Signal-to-Noise Ratio	Typical Transmission Coefficient	Typical V Value
Retarding Field	$5 \times 10^8 \, \frac{(k)}{\sigma} \left(\frac{s^2 \, T_R \, I_p \, V_p}{\eta B (V_p - V_A)} \right)^{1/2}$	1×10^{-2}	4×10^{-3}
127° Sector	$3 \times 10^8 \, \frac{(k)}{\sigma} \frac{(\Delta V)}{\sigma} \left(\frac{s^2 \, Ts I_p \, V_A}{\eta B \, \Delta V} \right)^{1/2}$	5×10^{-2}	2×10^{-3}
180° Mirror	$3 \times 10^8 \, \frac{(k)}{\sigma} \frac{(\Delta V)}{\sigma} \left(\frac{s^2 \, Tc \, I_p \, V_A}{\eta B \, \Delta V} \right)^{1/2}$	3×10^{-1}	10^{-3}

Each of the signal-to-noise ratios is physically reasonable and consistent. In the case of the retarding field analyzer, the S/N ratio is directly proportional to k (which is partially limited by the tolerable degree of non-linearity in the approximated Taylor expansion in eq (7), and inversely to σ. Bishop's experimental data[22] pointed out that in the retarding field method, the current in the second harmonic increases with k^2 up to $k = \sigma$, and flattens off to a constant value thereafter. In the case of the deflection method, the first harmonic

current increases linearly with k up to $k = 2\sigma/3$, then passes through a maximum, and when $k = 6\sigma$, the current goes down as $(k)^{-1/2}$. There is an optimum value in the electrostatic analyzers.

If V_A approaches V_p, then $V_p/(V_p - V_A)$ becomes very large. The other factors are intuitively reasonable. In the case of the electrostatic deflectors, in addition to the (k/σ) dependency, the S/N is also proportional to $(\Delta V/\sigma)$; the ΔV term arises from the limited signal arriving through the narrow slits. Furthermore S/N goes up as the 1/2 power of $(V_A/\Delta V)$.

The constants s and η are characterized by the sample under examination. The transmission coefficient T is governed by the geometry, with an absolute upper limit of 2π in the retrading analyzer, but much less with other analyzers. Any attempt to increase the T value may result in a loss of resolution. The bandwidth B can only be reduced to a reasonable limit beyond which the problem of drift and carbon build-up may become important. The latter problem arises from the long exposure of the focused beam on the sample surface resulting in a thin layer of carbon. This increasing carbon thickness will broaden and reduce the amplitude of the Auger peaks, and finally result in the total disappearance of the peaks. I_p cannot be increased indefinitely because the sample will heat up and contamination will build up too rapidly. These are some of the inherent factors limiting the S/N ratio attainable in practice.

To make some relative performance comparison, it is interesting to measure (S/N of sector)/(S/N of retrading field). Take some typical values such as $V_p = 2000$, $V_A = 500$, $\Delta V/\sigma = 1/2$, $k/\sigma = .4$ and .6 for

the sector and retarding field respectively ; then the quotient is approximately 10. Similarly, for the mirror analyzer, the guotient is 30 relative to the retarding field analyzer.

To reiterate the above discussion, it appears that most quantities (k, ΔV, I_p and B) governing the S/N of each analyzer have, in practice, been pushed to their limits. Ts and Tc cannot be increased much more, in line with reasonable resolutions. The only factor that can be pushed is T_R. This may be achieved by enlarging the retarding analyzer opening and incorporating spherical grids. A limiting 120° opening would increase T_R by a factor of nearly 100. This would put the S/N performance of the three detectors at a par with each other within a factor of three. It must be pointed out though that this enlarged aperture would create unwanted secondary electrons at the grids plus local variations in grid potential, and thus ultimately to some degradation of resolution.

As far as practical operation goes, the small retarding field analyzer is the easiest to use. It is compact and simple; no special technique is required for its installation. Care must be exercised in shielding the connection from the retarding grid to the power supply; otherwise stray fields may be created inadvertently. In contrast, the cylindrical mirror analyzer is more complicated and bulky. A magnetic shield is required to enclose the cylinder in order to minimize stray field perturbations.

In general, the electrostatic deflecting technique has at least one advantage over the retarding technique. That is, the former is always one derivative ahead of the latter. On the basis of theoretical considerations,

the 180° cylindrical mirror analyzer has the highest S/N performance, followed by the 127° sector and the retarding analyzer with the ratio of about 3:1:1, even when the aperture of the retrading analyzer is increased to the largest practical value. All three types should prove useful, and only extensive experience can determine which one will prove to be best in actual practice.

4 Characteristic Energy Losses

4.1 Introduction

When an electron with a given kinetic energy is incident upon the surface of a material, the energy is lost in varying degrees ranging from zero in an elastic collision at the surface to total absorption by the material.

If the energies of the electrons leaving the material, either after transmission through a thin film or reflection from a thick sample, are measured, a spectrum results with energies ranging from zero to almost the full energy before incidence. Two large peaks are found, one at each end of the spectrum. At the zero energy end are the secondary electrons and at the high energy end are the backscattered primary electrons, those which have lost little or no energy.

Along the spectrum certain other small peaks are found indicating certain energies are more common than others. Further, it is found that at various incident energies some peaks keep a constant relation to zero energy while other peaks keep a constant relation relative to the primary energy. The former are called Auger electrons and the latter are called characteristic loss electrons.

The origin of the characteristic losses is not clearly understood. Various theories have been proposed to explain the nature of these losses. The plasma oscillation, interband transition, and ionization theories will be discussed.

Various techniques have been employed to measure the characteristic energy losses. Most of the work has been done in the transmission mode

measuring the lower energy losses thought to be associated with the less firmly bound electrons in a metal.

This study was undertaken to establish techniques for measuring the higher energy losses thought to be associated with ionization of the more firmly bound electrons. In particular, the work was done in the reflection mode from a thick sample such as is commonly studied in the scanning electron microscope (SEM).

It was hoped that this work could help to provide the basis for the development of visualization and analysis techniques in SEM using characteristic loss peaks to identify materials on a microscopic level.

In addition it was the aim of the present work to improve our understanding of the physical nature of the loss peaks; that is, whether they are likely to be produced by plasma oscillations, interband transitions, or individual ionization processes of bound electrons in atoms.

4.1.1 History of Characteristic Energy Losses

The history of the characteristic energy loss summarized by Marton,[23] Leder, and Mendlowitz goes back to 1924 when J.A. Becker[24] reported work done with 200 eV electrons reflected from solids. He found practically no electrons losing energies in a range up to 11 eV, depending on the target. He did find electrons losing greater amounts of energy.

In 1927 D. Brown and R. Whiddington[25] reported similar results using a copper target.

E. Rudberg,[26] between 1929 and 1936, reported the first definitive investigations on, and coined the term, for characteristic energy losses. He clearly demonstrated that, when slow electrons impinge upon solid surfaces, there are characteristic values of energy losses forming a kind

of line spectrum of the energy distribution. He was able to show that the energy loss value depends only on the nature of the solid and not on the energy of the bombarding electrons up to an energy of 1 KeV.

Working at higher primary energies, G. Ruthemann[27] published reports between 1941 and 1948 on the observation of maxima in the energy spectrum of electrons after passing through thin layers of solids. He attempted to identify several of the energy losses which he called "discrete" with x-ray transitions. He observed, also, that certain losses occurred in integral multiples of a first, lower value, indicating that the same event was repeated in multiples.

The last two decades have seen considerable advances in the instrumentation and the measurement of the characteristic energy losses for the more common and available elements.

4.1.2 Interpretations of Characteristic Energy Losses

Several theories have been proposed to explain the origin of the characteristic energy losses. Much of the work done in the measurement of the loss spectra was undertaken in order to test these theories, as opposed to a straightforward measurement of the spectra.

An early theory proposed by Rudberg and Slater[28] in 1936 suggested that the interaction of the beam electrons and the atoms of the metal resulted in excitations of the valence or conduction electrons of the metal into higher allowed energy states. Since, in a solid metal, the initial and final states form energy bands, the theory describing these transitions is known as the Interband Theory.

Attempts have been made to correlate the characteristic energy losses with x-ray data as these also involve transitions of electrons into bands.

Richardson,[29] in 1930; Cuachois,[30] in 1952; and Leder[31] in 1956 have found some agreement between the characteristic losses and x-ray data. In a table of energy loss values by Klemperer and Shepherd[32] several losses are attributed to interband transitions. In the same table many losses are ascribed to ionization of the inner atomic shells. (Table 1)

A. Ia. Viatskin[33] has developed a comprehensive theory of the interband transitions in which the electrons are raised from the Fermi distribution of electron energy levels to the various Brillouin zones. He calculated the losses expected, the mean free path, the angular dispersion, and the effects of crystal structure and lattice constants. He found good agreement with experimental values, although he could not account for all the losses of some metals. He obtained an expression for the energy loss quantum which is given approximately by:

$$\overline{E}_n = h^2 n^2 / 2m \qquad (29)$$

where h is Planck's constant, n is the reciprocal lattice vector, and m is the effective mass of the lattice electron.

E.J. Sternglass,[34] in 1956, proposed a theory which considers the losses as being due to individual atomic excitation processes and to ionization processes leading to secondary emission. In this interpretation the characteristic loss peaks represent the ionization of the electrons in the bound shell next to the valence level, for which the binding energies range from about 10 to 20 eV for all elements. These electrons would leave the surface as secondary electrons with energies in a distribution with a peak amplitude at about 2 eV. The shape of the secondary distribution would determine the shape of the characteristic loss peak. This inter-

pretation fits the observations of Geiger in the noble gases and in mercury in the solid, liquid, and gaseous states. The results for the three states of mercury lead to the apparent conclusion that the losses must be occuring at the atomic level rather than as a collective electron action.

This theory also predicts that the energy losses for an element would remain almost constant when measured as a pure metal or as a compound with no free conduction electrons.

The theory of characteristic losses due to induced plasma oscillations in the Fermi gas in metals has prompted the majority of the work in measuring the energy losses. This theory has been accepted by most experimenters as the explanation behind the most prominent loss lines.

In the plasma loss theory, the incident electron is assumed to excite the Fermi gas as a whole, the electrons acting collectively. The energy transferred can occur only in integral multiples of an elementary quantum of energy, which is proportional to the circular frequency of the plasma oscillations.

The collectivity of the gas of free electrons can oscillate with a frequency, F_b, given by:

$$F_b = (n\, e^2 / m_o\, K)^{1/2} \qquad (30)$$

where n has integer values, e and m_o are the charge and mass of the electron and K is the dielectric constant. F_b would correspond to a bulk plasma energy loss by:

$$E_b = h\, F_b \qquad (31)$$

The plasma loss takes two forms, volume and surface. The volume loss is thought to be the most prominent loss line in the spectrum. Most metals

also exhibit a lower loss which is attributed to the surface plasma oscillation. The value of this surface plasma loss is given by:

$$E_s = E_b / (2)^{1/2} \qquad (32)$$

H. Raether[35] reviewed the experiments prior to 1965 and concludes that "The concept of Bohm and Pines that the characteristic energy losses of electrons have transmitted a solid are due to the excitations of oscillations of the electron plasma, has found excellent confirmation."

Even though most workers in this field of endeavor tend to agree with Raether, it should be noted that the plasma theory does have some difficulties explaining the energy losses. By this theory there should not be losses in insulators, however losses have been found in materials with no free electrons. The plasma theory does not explain the losses which have been measured for individual atoms in the gas or vapor phase, and the theory does not explain the shape of the observed loss peaks.

4.2. Theoretical

4.2.1 Review of Recent Literature

The majority of the work that has been performed in the last few years was initiated to test and attempt to verify the theory of plasma oscillations as the principal source of characteristic energy losses. Most authors have concluded that the lowest loss line is due to a surface plasma loss, and that the line with the largest amplitude is due to the volume plasma loss, while loss-lines at higher energies are generally interpreted as multiples of one or both of the former two losses.

Only a few investigators have reported loss lines at energies greater than approximately 30 eV. For this reason there have been few interpretations of losses caused by interband transitions or ionization.

According to the theory of plasma oscillations volume plasma losses generally lie in the region between 10-20 eV with surface losses between 7-14 eV. Ionization losses involving the more firmly bound electrons would occur at energies of greater than 20 eV for most elements although losses involving the loosely bound electrons could lie in the 3-10 eV range.

This study will concentrate primarily on those investigations which included measurements at the higher energies.

N. Swanson and C.J. Powell[36] report measurements of the excitation of L-shell electrons in Al and two forms of Al_2O_3. They obtained spectra for energy losses in Al with the dominant feature being the 15 eV peak assumed to be due to plasmon excitation and multiples at 30,45, and 60 eV successively diminishing in intensity. At about 72 eV there is an increase in energy-loss intensity associated with the excitation of the L-shell electrons. This loss is believed to correspond to measured x-ray absorption at 72.7 eV.

They also report four other losses for which x-ray absorption have been measured. These are at 76, 96, 111, and 124 eV. The 111 eV line had been measured by H. Watanabe[37] and attributed to a combination of the 96 eV and the 15 eV plasmon loss. However, Swanson and Powell[38] show a weak peak at 111 eV after the characteristic loss contribution is subtracted.

Swanson and Powell report five measured losses on Al_2O_3 which correspond to x-ray absorptions. These are at 76, 77, 79,98, and 123 eV. They also found apparent plasma losses at 23 and 46 eV.

They attempted to measure ionization cross sections using the spectra obtained by bombardment with an electron beam. They found that the cross

sections of ionization of inner shell electrons in solids can be measured more directly by this technique then by finding the yield of x-rays following the decay of the particular excited state. This is accomplished by comparing peak amplitudes from the ionization losses with the amplitude of a peak of known cross section.

Concluded from the study was that structure observed in the electron energy loss spectra corresponding to L-shell excitation in Al and Al_2O_3 is in good agreement with structure observed in soft x-ray absorption measurements on the same materials. In their measurements of the ionization cross section, they found the total cross section per Al atom for L-shell excitation to be about one-fourth of that for the loss at 15 eV generally regarded as due to plasmon excitation.

V.V. Rumyantsev (39) reports on the problem of line shape for the maxima in the energy spectrum of electrons scattered in solids with characteristic energy losses. He determines the shape of the loss line from theoretical considerations.

He finds that the relative height of the plasmon peak with respect to the part of the spectrum formed by electron-electron collisions depends considerably upon the energy of the fast particles. The fact that the line shape of the plasmon peak is a function of the primary energy can be used to separate the experimental spectra into lines corresponding to plasma losses and lines whose form is mainly determined by the excitations of of electrons.

J. Thirlwell (40) experimented with Al and Cu and found that both the surface and volume plasma losses of Al cease to be excited when the primary energy is less than about 26-29 eV, the surface loss cutting off at a

slightly lower primary energy than the volume loss. The remainder of his paper is concerned with verifying the values of the plasma losses. He found a problem of conflicting results for Cu in that there is no general agreement as to which of the energy losses observed are due to the excitation of plasma oscillations.

R.E. Burge and D.L. Misell (41) show that the electron energy loss distributions observed in electron transmission through Al films may be fitted to predicted values in the energy ranges from 5 to 100 eV within a deviation of a few percent. The fitting is made in terms of assumed electron energy loss distributions for the principal volume and surface losses which are centered at about 15 and 7 eV. Consistent values of the mean free path for elastic electron scattering are evaluated for six primary energies from 23 KeV to 70 KeV.

Burge and Misell found good agreement with distributions of the various peaks as predicted by the plasma theory at loss energies below about 70 eV. Their mean free path calculations were also in agreement at the lower energies.

They conclude that the difference between the calculated and experimental curves at high energies is greater than could possibly be accounted for by any effects due to angular redistribution of the electrons scattered by the plasma processes. A similar discrepancy above a given value of energy loss was found for carbon. They state that the discrepancies are probably due to single electron processes, such as interband transitions and ionization.

It should be noted that the report by Swanson and Powell discussed earlier found ionization losses beginning at 72 eV and the observations of Burge and Misell support the plasma theory up to an energy of about 70 eV.

G.C. Hale and J.B. Hasted[42] measured the characteristic energy loss of electrons transmitted through Argon. They found loss peaks at 245 and 247 eV corresponding to L-shell x-ray edges, at about 12 eV corresponding to M-shell excitation and ionization, and at 256-258 eV resulting from simultaneous ionization of L and M electrons. They also found a peak at 230 eV but only when scattered at zero degrees. They submit that this peak could be caused by the collective excitation of a number of electrons.

M.J. Lynch and J.B. Swan[43] measured energy loss spectra for the second and third transition metals.

They report that the plasma theory has had considerable success when applied to experimental observations of several of the transition elements, but that for many other cases a modification to the theory is required in order to obtain satisfactory agreement with experiments. The modifications involve which electrons are considered free and which are considered bound.

The second and third transition groups consist of ten elements each of which Lynch and Swan measured losses for seven and six elements respectively. (Table 3) They found good agreement between the plasma theory and their measured plasmon loss for the first four elements of each group. However the measured loss values for four elements were one to six volts lower than the predicted values from the theory assuming all s and d electrons are free.

In addition to the plasmon losses a total of 22 peaks ranging from about 25 to 70 eV were measured for the various metals. These energies correspond well with the known ionization energies of the metals.

Their interpretation of the loss peaks in terms of ionization processes is supported by measurements made to the point of inflexion of the

ionization loss, that is, to the lower energy edge of the peak rather than to the intensity maxima.

They conclude that for all metals studied one peak in each spectrum is identified with high likelihood as arising from volume plasmon excitation and another peak is ascribed to surface plasmon excitation. On the basis of reasonable energy agreement and appearance, other peaks are associated with ionization processes occuring in identifiable atomic subshells.

They also found a set of broad intense peaks in each group which has been assigned a common but unidentified origin.

4.2.2 Correlation Between Characteristic Losses in Ionization Potential

While reviewing the literature for characteristic energy losses, an apparent association between the loss values and the work function for the same element was noted. This association was investigated by plotting the loss values attributed to plasma losses versus the work function. The loss values were taken from Klemperer and Shepherd's[44] article which has the latest available compilation of characteristic loss values. These values were supplemented by values reported by Lynch and Swan.[45]

Figure 11 shows the results obtained for thirty elements. The calculated correlation coefficient is 0.656 with a t value of 4.51. This means that, with a probability of greater than 0.995, there is a true positive correlation.

Since the listed values of the work function vary and since there is a correlation between the work function and the ionization potential for an element, a plot was made of the listed plasma loss value versus the ionization potential.

This relationship is shown in Figure 12. The correlation coefficient for this data is 0.622 with a t value of 4.55. Again, with a probability of greater than 0.995, there is a positive correlation between the ionization potential and the measured characteristic loss.

Klemperer and Shepherd list several loss values for each element and attempt to identify each loss as either surface or bulk plasma losses and multiples, interband transitions, or ionizations.

On a plot of all the losses for all the available elements versus the ionization potential, apparent trends were noted. Two examples are presented in Figure 13.

Loss values for K, Ca, Ga, Ge, As, and Se are plotted in the upper part of Fig. 13 (marked (a)). These elements are in the fourth period of the periodic table and have valence electrons in either the 4s or 4p subshells.

The listed values for Ga, Ge, and Se are assigned the origin of a double plasma loss by Klemperer and Shepherd. They assign an ionization of an M electron for the Ca loss and they do not explain the losses for K and As. However, x-ray absorption measurements for K and As are 4 and 1 eV, respectively, below the measured losses. It could be assumed therefore that the losses for Ca, K, and As are all ionization losses. If this assumption is true, then it is difficult to explain the correlation between plasma losses for three of the six and ionziation losses for the other three. A conclusion that appears reasonable is that all six are really ionization losses.

In the lower part of Figure 13, loss values for In, Zr, Mo, Rh, Pd, Sb, and Te are plotted versus the ionization potential. These elements

are all in the fifth period of the periodic table (b). The losses for the first five are explained in the literature by a single bulk plasma loss and the last two losses are assigned a combination of a surface and a bulk plasma loss.

Considering the high correlation, calculated to be 0.975 for all seven elements, it seems difficult to believe that the origins are not the same. However common origins for these seven losses cannot fit the present plasma theory, and strongly suggest a fundamental connection with the ionization of an outer atomic shell.

That such an interpretation of the dominant losses fits the hypothesis that the principal loss-peak typically lying between 7 and 25 eV for all elements is probably associated with the ionization process leading to the ejection of a secondary electron is particularly clearly brought out by the loss spectra for mercury vapor, liquid and solids shown in Fig. 14.

For the case of the free atom, the peak is seen to lie about 1 eV above the known ionization potential of 10.42 ev, corresponding to the fact that the most probable energy carried away by secondary electrons is of the order of 0.5-2.0 ev for a number of gases. In the case of solid mercury, the peak is shifted to slightly higher energies, consistent with the fact that for most metals, the most probable secondary electron energy tends to be somewhat higher, typically between 1 to 3 ev. The loss peak corresponding to ionization is broadened and the lower-lying discrete loss produced by excitation to a narrow final state in the free atom is washed out, corresponding to the well-known broadening of discrete atomic levels into bands in the solid.

Based on this process of secondary electron formation from the outermost filled shell, the observed data on the position of the principal loss peak for the rare gases Xe, Kr, A and Ne shown in Fig. 15 is very simply understood. In all cases, it lies within 2ev above the ionization potential as indicated by the lower of the two diagonal lines shown in Fig. 15. Not only the rare gases with their filled shells fall into this pattern, but also the metals Ag and Hg, suggesting that this particular loss is probably also associated with an ionization process.

If one now examines the table of characteristic losses given by Klemperer for other elements, one finds that for all the metals listed there exists the same simple relationship to the known ionization potential of the free atom as observed for the rare gases as well as for Ag and Hg above. In every case, one of the prominent loss peaks listed in the energy range between 5 and 13 ev occurs within 3 ev of the ionization potential, as shown in Fig. 16.

In fact, the majority of the elements fall on a parallel line to that representing the ionization potential that is spaced exactly 3 ev higher to within the accuracy with which the characteristic losses have been measured. Out of the 12 elements K, Li, Na, Ba, Al, Ca, Cr, Mu, Mg, Ag, Be and Hg, only Na, Ba, Al and Ag have loss peaks closer than 3 ev above the ionization potential, and none lies outside the narrow 3 ev wide zone.

As to the losses above about 13 ev and below 25 ev reported for a number of elements, one might expect these to correspond to the ionization of the next deeper lying atomic shell. This expectation is seen to be

confirmed by inspection of Figure 17 where the binding energies of all the outermost atomic shells with energies below 65 eV have been plotted together with the well established characteristic losses and the ionization potentials for the elements up to Z = 50.

Inspection of Fig. 17 shows that to a remarkable extent, all except one or two of the observed characteristic losses between 7 ev and 35 ev do indeed fall within about 3 ev above the known binding energy of one of the outer shells wherever these are known. And in the cases where the binding energies are not accurately known, as for instance for the 3d shell between Z = 21 and 32 where Fe, Co, Ni, Cu and Zn are located, the observed losses lie at energies that are consistent with the likely position of the 3d levels. Thus, x-ray photo-emission studies have recently suggested a 3d binding energy for Zn of 9 ev below the Fermi level, or about 13 $\pm$ 1 ev below the vacuum level, in good agreement with a characteristic loss value of 14 ev as shown in Fig. 17. One can turn the argument around and say that the characteristic loss measurements seem to give the most direct measurements of the likely position of the 3d band for these atoms yet available.

Since the remaining characteristic levels above 25 ev have either been explained as multiple occurrences of the lower lying losses or as ionization of still deeper lying shells, there seems to be no case left where one is forced to postulate a plasma loss as the only possible explanation.

Even the well-known sharp loss peak for Aluminum near 15 ev generally cited as the strongest confirmation of a collective loss mechanism is seen to lie just 3 ev above the 3s shell binding energy of 12 ev, exactly where it should occur between Mg and Si.

Only in the region below about 5 to 7 ev, corresponding to the optical excitation of free atoms, does the collective excitation of the conduction electrons appear to be involved in the characteristic loss process. This energy range corresponds to the region where the optical theory of metals dominates, and where the energy is generally insufficient to lead to removal of any significant number of electrons from the metal by a secondary emission process.

This is in fact the region where the band-model of solids has been most successful, and the optical theory of collective electron behavior should apply.

But it now seems that as far as the more energetic characteristic loss processes are concerned, these seem to be satisfactorily explained in terms of individual electron-electron collision processes leading to the formation of secondary electrons.

The fact that the losses in the 5 to 15 eV energy region are so closely associated with the ionization energy of the free atom even in solids is a very surprising result that may turn out to have important consequences for the nature of the interaction mechanism of fast electron with matter and our ideas as to changes that take place when materials undergo phase transitions.

If the electron-electron interpretation of the principal characteristic loss processes above 5 ev is correct, then a detailed study of these losses in free and bound atoms should be extremely valuable in studying the changes in the binding energies of molecules and solids. This would supplement other techniques such as the x-ray induced emission of photo-electrons developed by Siegbahn (46) recently applied to the study of Zn and its compounds cited above. Furthermore, a precision measurement of these

losses could serve to identify the particular chemical atom in the same way as the characteristic x-rays and Auger electrons produced by the ionization of much deeper lying shells.

This would open up a valuable new analytic technique particularly suitable for use in a scanning electron microscope equipped with an efficient electron velocity analyzer. The advantage is the much greater intensity independent of atomic number and the possibility of precise positioning made possible by a finely focused electron beam as contrasted with a beam of soft x-rays that cannot be deflected.

The successful development of high efficiency velocity analyzers suitable for use in the SEM should therefore prove to be of considerable value in the study of the deeper lying outer electronic states of solids and molecules than those accessible by ordinary optical techniques.

4.3 Experimental Techniques

The instrumentation used to measure characteristic energy losses depends on the mode of operation, that is, transmission or reflection.

In transmission experiments, the electron beam is passed through a thin film of the sample and then the spectrum is determined. The most popular energy analyzer that has been used in transmission work is the Mollenstedt type. This analyzer is easily adapted to transmission electron microscopes. The analyzer is essentially an electrostatic saddle-field lens of very strong chromatic aberration. A parallel beam of heterogeneous electron energies emerging from the exit side of a thin foil enters the electrostatic field at some distance from the axis and the electrons with different energies are deflected by varying amounts. In the microscope, these deflections are magnified by the projection lens and are then focused onto a

fluorescent screen or a photographic plate. A resolution of up to 1 in 70,000 has been achieved with the Mollenstedt analyzer.

The group doing most of the recent work in reflected characteristic energy loss measurements on reflected electrons from thick targets, namely Powell, Robins, and Swan[47] used a simple focusing 127° electrostatic analyzer. In this type of analyzer, the electrons enter a slit and then move into a uniform electrostatic field between two parallel plates forming an arc of 127°. They pass through another slit at the exit end and are detected by an electron multiplier. As the potential between the two plates is varied, electrons with different velocites follow different paths such that the various radii of curvature allow only discrete energies to pass through the second slit. The entire spectrum may be analyzed by continuously varying the voltage applied to the curved plates.

Some groups measuring reflected electrons have used a retarding potential method. This involved applying a negative potential to a grid through which the electrons must pass before being detected. As the opposing potential is increased only those electrons with energies greater than the opposing field will pass through the grid. The spectrum obtained with this method is an integrated spectrum, that is, the intensity reflects the number of electrons with energies greater than the applied potential.

In a theoretical consideration, A. Huen[48] has shown that for electrons leaving a surface in a divergent manner, which would be the situation with reflected electrons, a coaxial cylindrical analyzer is more efficient than either a retarding potential or a 127° analyzer by at least a factor of three. Therefore, a study was undertaken to demonstrate that a cylindrical analyzer can also be utilized in the SEM to measure characteristic energy losses with greater efficiency than other analyzers.

4.3.1 Cylindrical Analyzer

The coaxial cylindrical capacitor analyzer described by G.A. Harrower [49] was redesigned and built to fit into the SEM chamber. The sample is located on the coaxis of the two cylinders and the primary beam is incident such that the scattered electrons eminate from the sample at the axis. The electrons travel from the sample through a slit which is cut around the inner cylinder. Since both the sample and inner cylinder are at ground potential the electrons follow a straight line inside the inner cylinder. The optimum angle for the electrons is 42.3° measured from the axis.

The determining factor in the resolution with the cylindrical analyzer is the slit width. An optimum must be realized in that a narrow slit gives better resolution but decreases the solid angle of acceptance thus decreasing the signal-to-noise ratio. A theoretical value for the resolution of the detector used in this study is 0.1%. However, with the application of a ten volt AC voltage to the DC voltage, it is believed that the resolution is more nearly 0.2 to 0.3%.

When a negative potential is applied to the outer cylinder a retarding electrostatic field is established between the cylinders. This field causes the electrons to be deflected back into the inner field free region through the exit slit. For a specific applied potential, only electrons of a specific energy will follow the required trajectory to reach the exit slit. By varying the applied potential, the entire electron spectrum may be caused to pass through the slit. After passing through the exit slit, the electrons are accelerated by a 10,000 volt potential and strike the scintillator.

4.3.2 Detection and Recording of Spectrum

As in the study of the Auger peaks described earlier, the DC potential applied to the cylindrical analyzer was modulated at one kilohertz with a peak-to-peak modulation of ten volts. This same AC signal was also applied as the reference signal to the phase-lock amplifier.

4.3.3 Measured Characteristic Energy Losses in Aluminum

The aluminum sample in the form of a one centimeter diameter disk of 99.9% purity was scraped prior to insertion in the chamber in an attempt to remove the aluminum oxide layer. It is known, however, that a thin oxide layer of about 10-20 Å remains even after this treatment.

Figure 18 shows typical spectrum for two primary energies, 1 and 1.2 KV. Since the amplitude of the characterisitc energy loss peaks is not much greater than the noise peaks, multiple runs were made to determine which peaks were observed constantly as opposed to peaks that occured only in one run.

Table 4 lists the measured energy losses. In column (a) for a primary energy of 1000 eV, nine peaks are listed which were reproducable in multiple runs. Column (b) lists six values obtained with a primary energy of 1200 eV. The six values at the higher energy correspond within 2 Ev of six of the peaks at the lower primary energy. This is one determining feature of the characteristic energy losses; that is, the value of the loss is independent of the primary energy.

Further evidence that the measured peaks are characteristic energy losses is obtained by comparing the loss values with the loss values measured by Swanson and Powell[50]. Table 5 shows the comparison of the two sets of data with the measured x-ray absorptions. The first four values

measured by Swanson and Powell; 15, 30, 45, and 60;are explained by them as the plasma loss and multiples thereof. The peak at 15 eV was not found in the present work. A possible explanation is that this peak would lie on the part of the spectrum that is undergoing very rapid change and therefore the peak is hidden in the background of backscattered electrons.

There is good correlation between the two sets at values of 73, 97, 112, and 124 eV. In the present work no peak was found at 77 eV. However, a peak was measured at 85 eV in the present work but was not found in the former work. This peak corresponds to a known x-ray absorption energy. A peak at 82 eV has been measured by Watanabe.[51]

4.4 Conclusion

The current work has demonstrated the feasibility of measuring characteristic energy losses in the SEM system using a cylindrical analyzer. For aluminum, agreement was found between characteristic loss measurements taken at two primary energies and the observed peak positions agreed with measurements made by other investigators.

It is believed that with further work it will be possible to obtain an energy loss spectrum in a few seconds as compared to the present two minutes. This, combined with the possibility of obtaining an image of the sample through the analyzer using the SEM, would allow a qualitative analysis of small sections of a sample.

It has been shown that there exists a correlation between measured characteristic losses and the binding energies of the outermost atomic shells. It is believed that further detailed studies of these losses in free and bound atoms could lead to a much deeper understanding of chemical bonding and the structure of the outer electronic shells in solids.

The scanning electron micrsocope therefore has demonstrated once again its unique capacity to obtain not only structural but also new forms of analytical information on a microscale not readily attainable by any other instrument.

5.0 SEM Auger Detector Prototype

5.1 Auger Analyzer Operating Instructions

A. Procedures for Producing a DC Curve

Step 1: The electron beam is focused on the specimen, in the vicinity of the incremental area to be analyzed, in the conventional manner. The electron beam scanning circuit should now be disabled and the magnification increased to a high value.

Step 2: Disconnect the video signal cable connecting the Photomultiplier assembly and the Video Control chassis. Connect a new cable between the Photomultiplier Assembly and the Input connector on the Keithley Electrometer. Set the Keithley range switch to obtain an on scale reading, then alter the position of the Auger Detector until a maximum output reading is noted on the Keithley electrometer.

Step 3: Place the AC Power On/Off Switch in the On position. This switch is located on the front pannel of the Auger Analyzer Control panel. This power switch will also apply AC power to Hewlitt-Packard Model 201 B audio Oscillator and the P.A.R. Phase Lock Amplifier.

Step 4: Set the Slope switch, on the Auger Analyzer Control chassis, to its middle or disconnected position.

Step 5: Place the Voltmeter Range Switch to the 5000V position.

Step 6: Turn the Sweep Mode Switch fully clockwise to the Set Sweep position, then place the Set Sweep switch in the desired rate position.

Step 7: Connect the proper cable between the X-Recorder Out jack, on the auger analyzer control chassis, and the X-In connection on the X-Y Recorder.

Step 8: Connect the proper cable between the Amplifier Out connector, on the back of the Keithley electrometer, and the Y-In connector on the X-Y Recorder.

Step 9: The X-Y Recorder should now be calibrated in accordance with the manufacturer's instructions.

Step 10: Set the Slope switch to the fully counter clockwise or Up position. The analyzer will now begin to program itself to maximum potential in accordance with the Set Sweep Rate determined in Step 6.

Step 11: Once the full output of the ramp voltage has been reached, place the Sweep Mode switch in the Center or Reset position. Now place the Slope switch in the Clockwide or Down position and the analyzer potential will quickly sweep back to a zero volts indication completing one Auger DC spectrum.

Step 12: Reset the Slope switch to the center disconnected position and the Sweep Mode switch to the Set Sweep position in preparation for the next run.

B. Procedures for Producing a Derivative Curve

Step 1: Repeat instructions given in steps 1 through 7 of section A on procedures for producing a DC curve.

Step 2: Connect a cable between the Photomultiplier Assembly Signal Out Put Connector, and the Channel A input connector on the pre-amp of the P.S.R. Lock In Amplifier. Assure that the input Channel Selector Switch on the preamplifier is in the Chan A position.

Step 3: Connect a cable between the Hewlitt-Packard Audio Oscillator and the Ref In/Out connector on the P.A.R. Lock In Amplifier using a BNC TEE connector.

Step 4: Connect a cable between the OSC In connector, on the bottom panel of the electronics rack, and the BNC TEE connector on the P.A.R. Lock In Amplifier REF In/Out connector.

Step 5: Place the Meter Monitor switch in the REF position.

Step 6: Tune the Hewlitt Packard Audio Oscillator to a frequency of 400 hertz.

Step 7: Tune the frequency of the P.A.R. Lock In Amplifier to 400 hertz using the Frequency Range switch and Vernier Dial.

Step 8: Peak the signal reading on the P.A.R. front panel meter by adjusting the frequency of the P.A.R.

Step 9: After peaking the REF signal, adjust the peak signal level to be between 1.0 and 1.5 on the meter scale by using either the Amplitude control on the Audio oscillator or the REF Attenuator control on the P.A.R. front panel.

Step 10: Place the Meter Monitor switch, on the P.A.R., in the Mixer position.

Step 11: Set the P.A.R. Sensitivity control to about the 10 MV position.

Step 12: Using the Phase switch and the 0° to 100° Phase Shift Vernier, attempt to obtain a zero state reading on the panel meter at a fairly high sensitivity. Then set the Phase Shift switch to a position $\pm$ 90° from the null setting depending upon which direction the signal swing is desired.

Step 13: Place the Meter Monitor switch into the SIG position.

Step 14: The Sensitivity control on the P.A.R. Amplifier can be adjusted to the point where the red overload lamp is illuminated then reduced until the system is no longer overloaded.

Step 15: Connect the proper cable from the Y Record Out connector on the front panel to the Auger Analyzer Control Chassis.

Step 16: The conditions for the production of the first derivative curve are then the same as steps 9 through 12 of the DC curve produced in Procedure A.

(Note: During the performance of the run it may be necessary to change the Time Constant settting on the P.A.R. Amplifier to obtain a reasonable amount of discernable information from the trace).

5.2 Circuit Diagrams

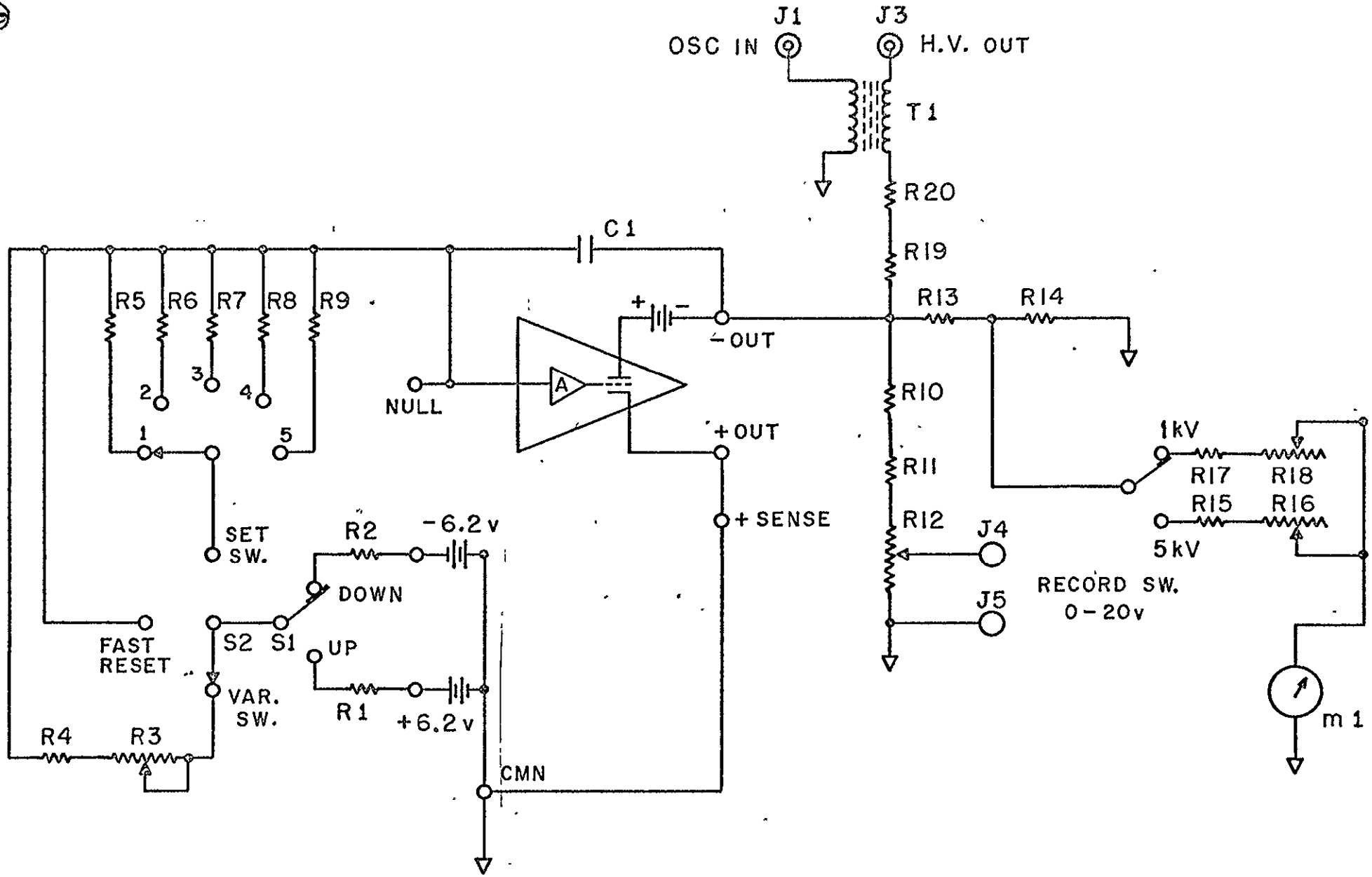
J1
OSC IN
J3
H.V. OUT
T1
R20
R19
C1
R5
R6
R7
R8
R9
R13
R14
+
−
−OUT
2
3
4
NULL
A
R10
1
5
+OUT
1kV
R17
R18
R11
R15
R16
SET
SW.
R2
−6.2v
+ SENSE
R12
J4
5kV
DOWN
RECORD SW.
0−20v
J5
FAST
RESET
S2
S1
UP
VAR.
SW.
R1
+6.2v
m1
R4
R3
CMN

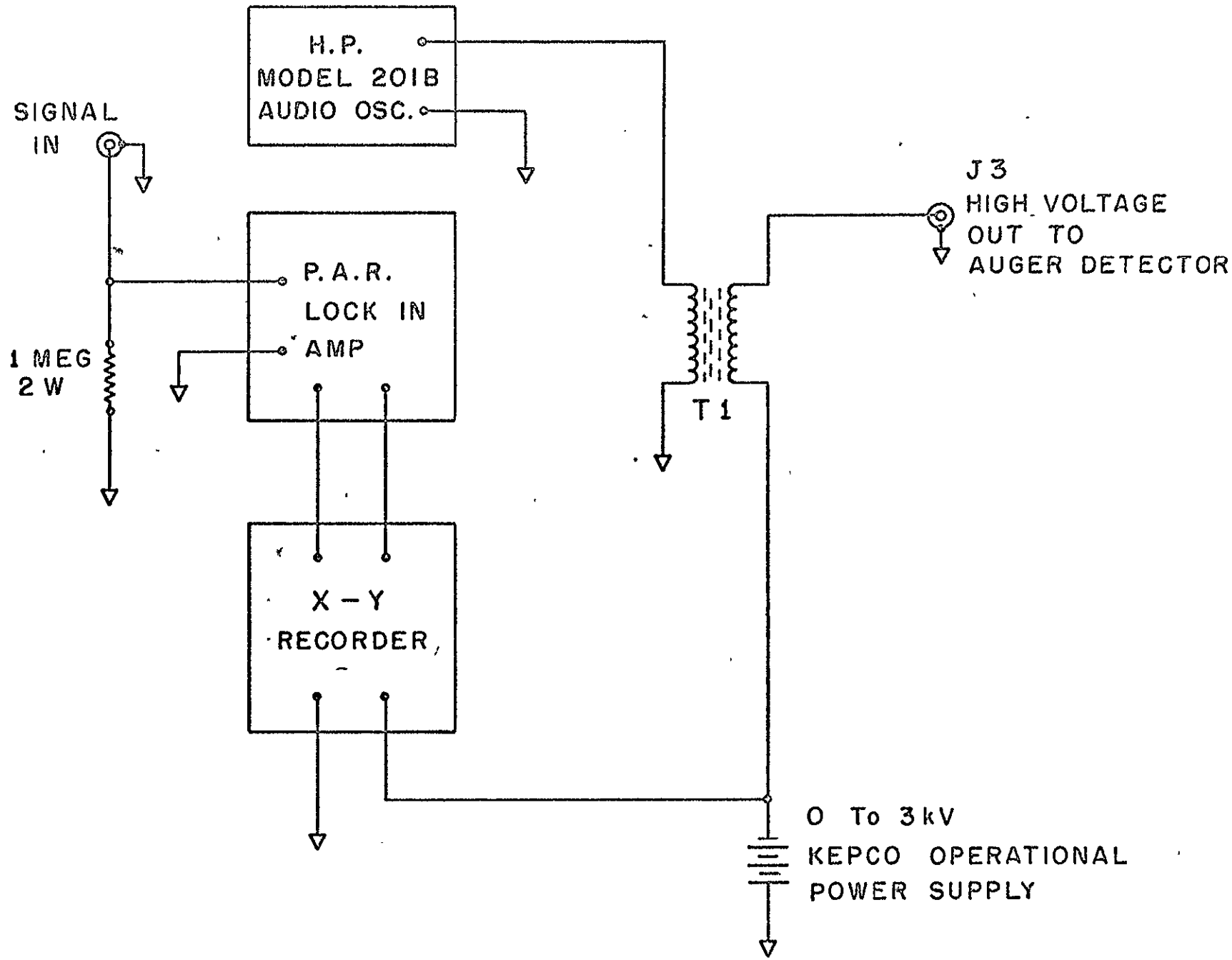
H.P.
MODEL 201B
AUDIO OSC.
SIGNAL
IN
P.A.R.
LOCK IN
AMP
1 MEG
2 W
X – Y
RECORDER
J 3
HIGH VOLTAGE
OUT TO
AUGER DETECTOR
T 1
0 To 3 kV
KEPCO OPERATIONAL
POWER SUPPLY

5.3 Detector Drawings

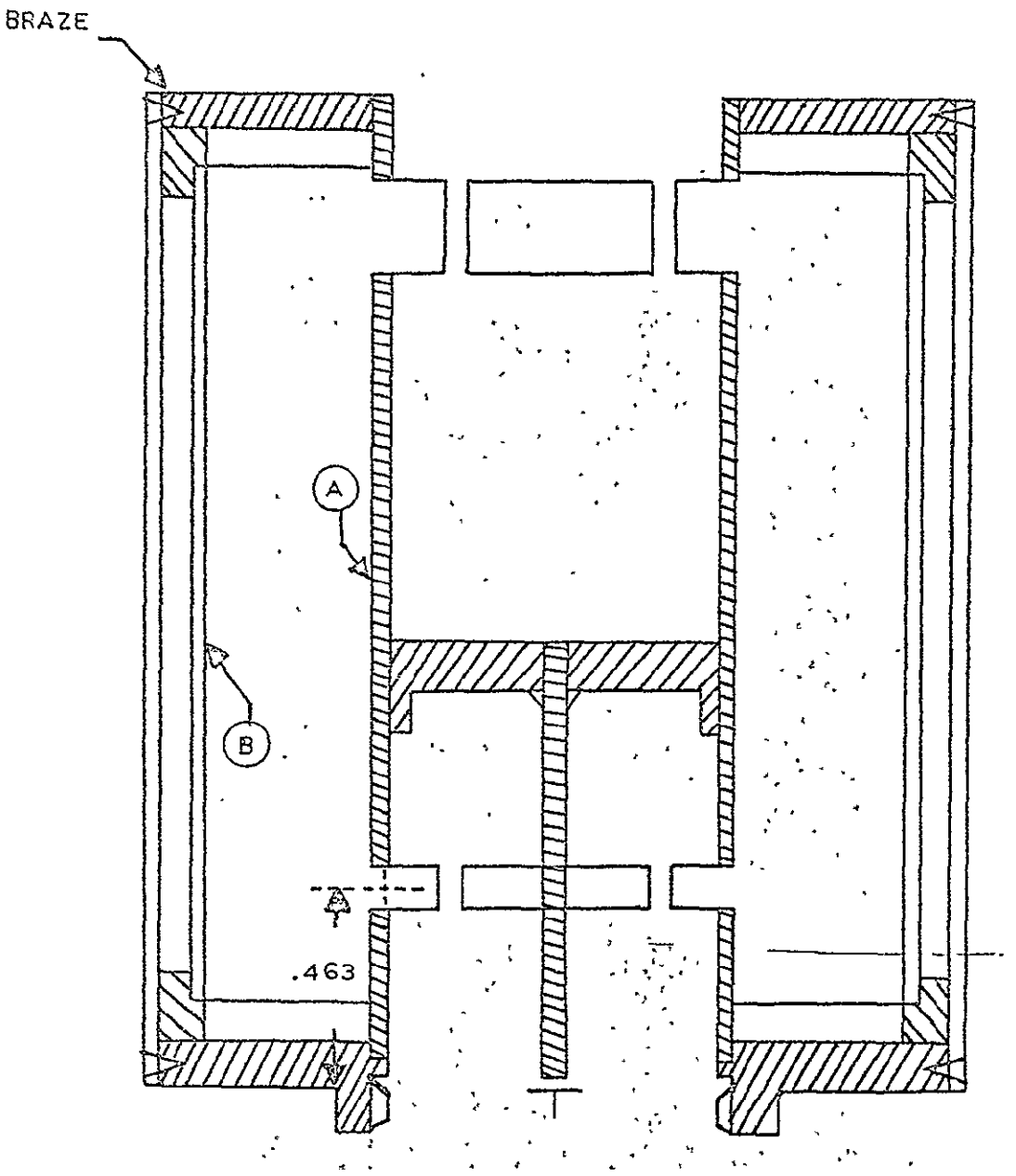

CYLINDRICAL
AUGER
ANALYZER

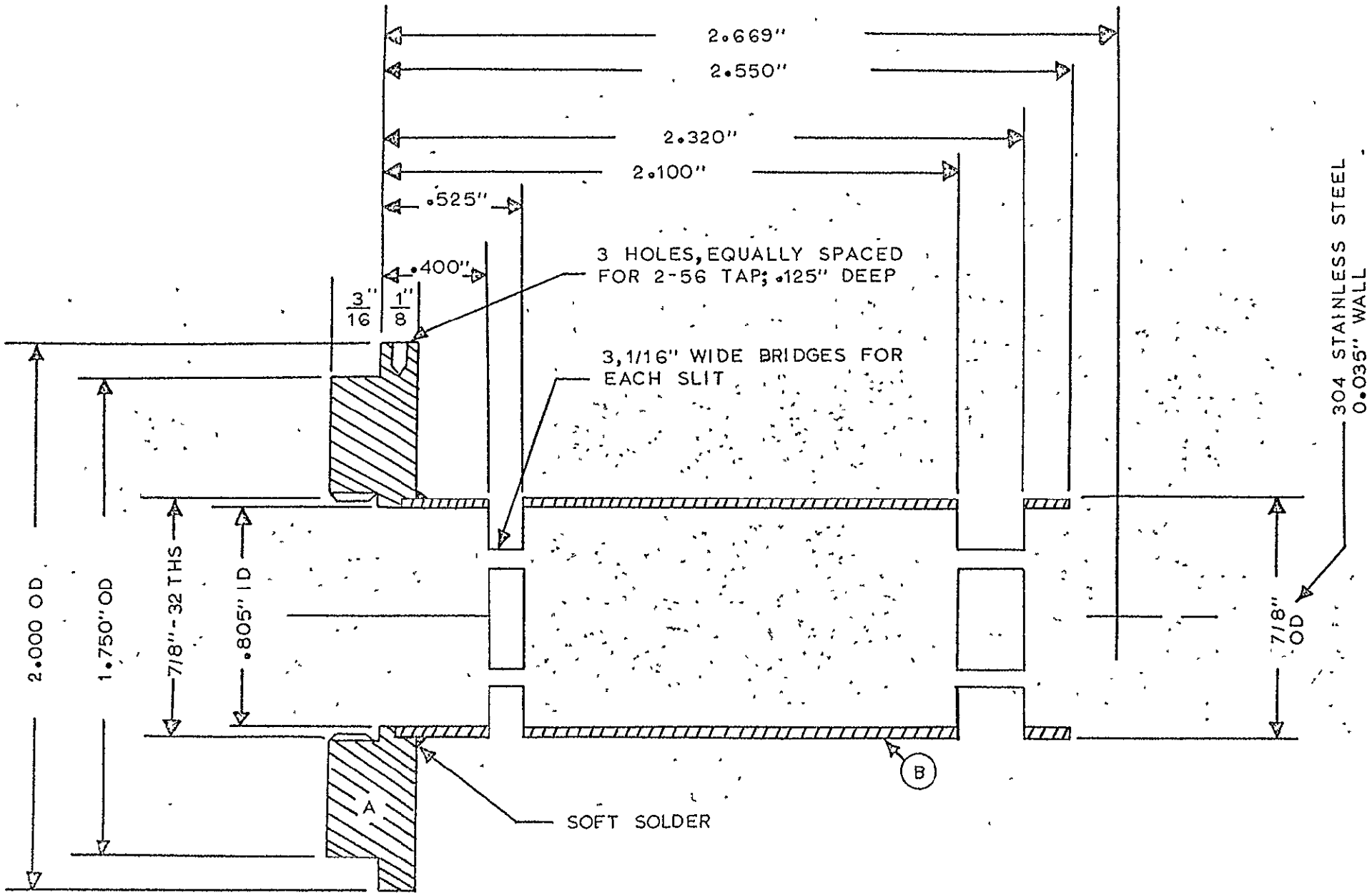

ITEM A : COLD ROLL STEEL

ITEM B : 304 STAINLESS STEEL

CYLINDRICAL ANALYZER

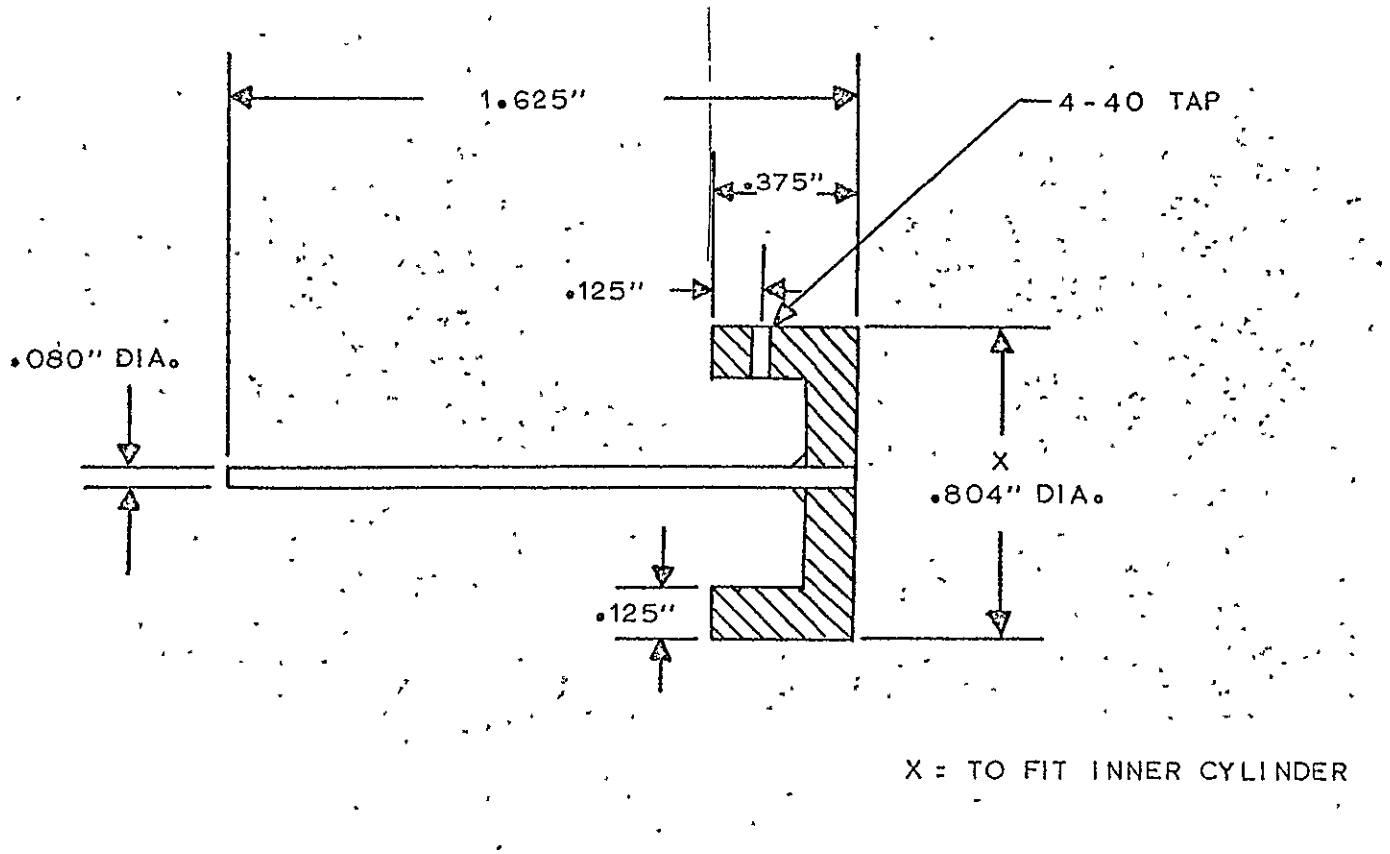

CYLINDRICAL ANALYZER

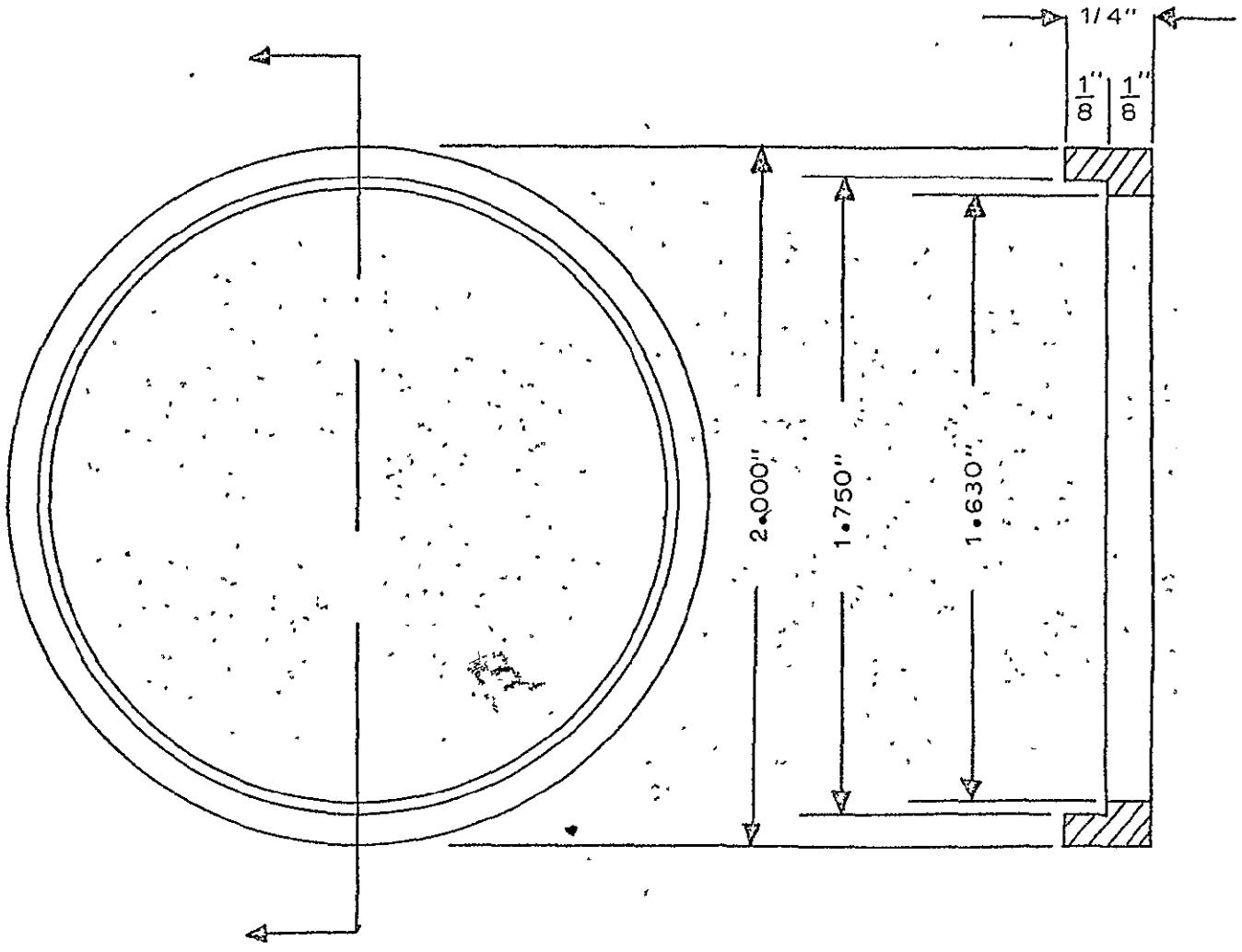

TEFLON

TWO REQUIRED WITH DEMENSIONS TO FIT STANDARD CYLINDER

5.4 Parts List

AUGER ANALYZER		
PARTS LISTING		
ITEM NO.	CALL OUT	DESCRIPTION
1	R1	Resistor, 7 Kohm, 1W, 5% Carbon
2	R2	Resistor, 7 Kohm, 1W, 5% Carbon
3	R3	Potentiometer, 2 Meg, 1 turn, 2W
4	R4	Resistor, 20 Kohm, 1W, 5% Carbon
5	R5	Resistor, 43 Kohm, 1W, 5% Carbon
6	R6	Resistor, 200 Kohm, 1W, 5% Carbon
7	R7	Resistor, 430 Kohm, 1W, 5% Carbon
8	R8	Resistor, 2 Meg, 1W, 5% Carbon
9	R9	Resistor, 5.1 Meg, 1W, 5% Carbon
10	R10	Resistor, 1 Meg, 2W, 5% Carbon
11	R11	Resistor, 1 Meg, 2W, 5% Carbon
12	R12	Potentiometer, 75 Kohm, 1 turn, 2W
13	R13	Resistor, 1 Meg, 2W, 5% Carbon
14	R14	Resistor, 1 Meg, 2W, 5% Carbon
15	R15	Resistor, 2 Meg, 2W, 5% Carbon
16	R16	Potentiometer, 1 Meg, 1 turn, 2W
17	R17	Resistor, 501 Kohm, 2W, 5% Carbon
18	R18	Potentiometer, 3 Meg, 1 turn, 2W
19	R19	Resistor, 1 Meg, 2W, 5% Carbon
20	R20	Resistor, 1 Meg, 2W, 5% Carbon
21	C1	Capacitor, oil filled, 2 MFD, 3,000WVDC
22	T1	Transformer, Thordarson Model 24R02U
23	M1	DC Voltmeter, 1 ma FS deflection
24	J1	Connector, panel mount; Amphenol UG 957/U
25	J2	Connector, panel mount; Amphenol UG 957/U
26	J3	Connector, High Volts; Amphenol UG 931/U
27	J4	Banana Plug Jack, Panel Mount
28	J5	Banana Plug Jack, Panel Mount
29	S1	5 position rotary switch, single pole
30	S2	5 position rotary switch, single pole
31	S3	5 position rotary switch, 3 pole
32	S4	5 position rotary switch, single pole

6. Tables and Figures

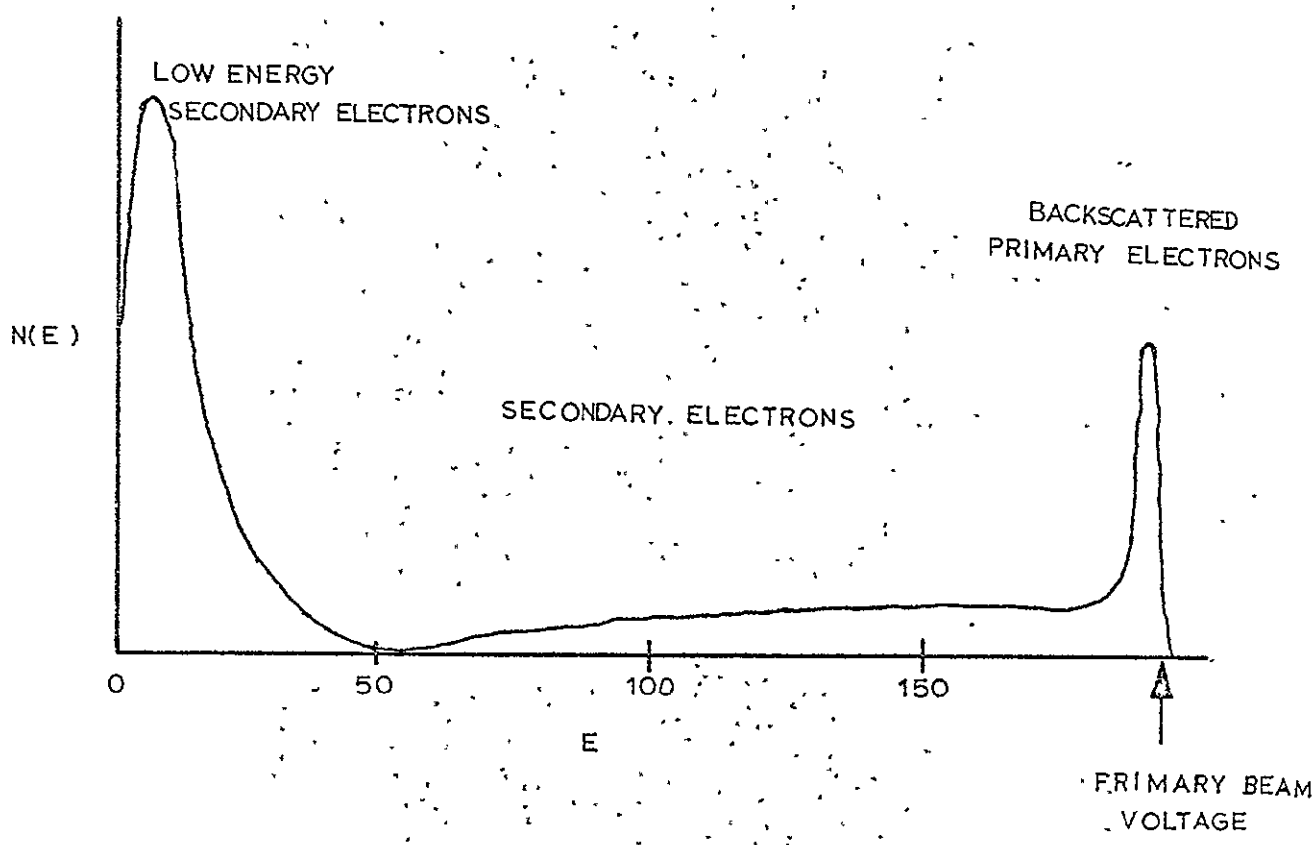

FIGURE 1

AN EXAMPLE OF SECONDARY ELECTRONS ENERGY SPECTRUM

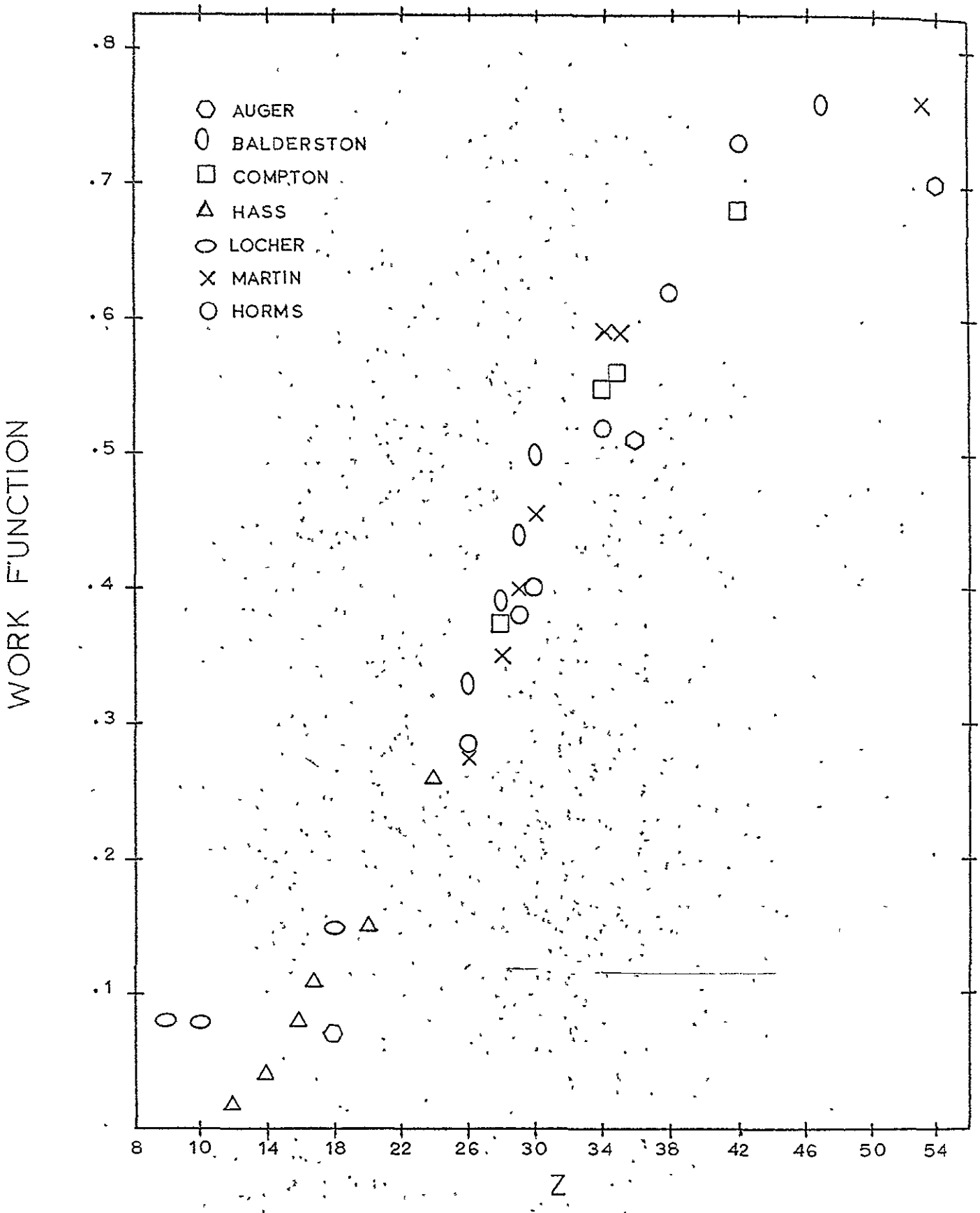

FIGURE 2

VALUES OF THE FLUORESCENCE YIELD FROM THE K LEVEL ACCORDING TO VARIOUS OBSERVERS

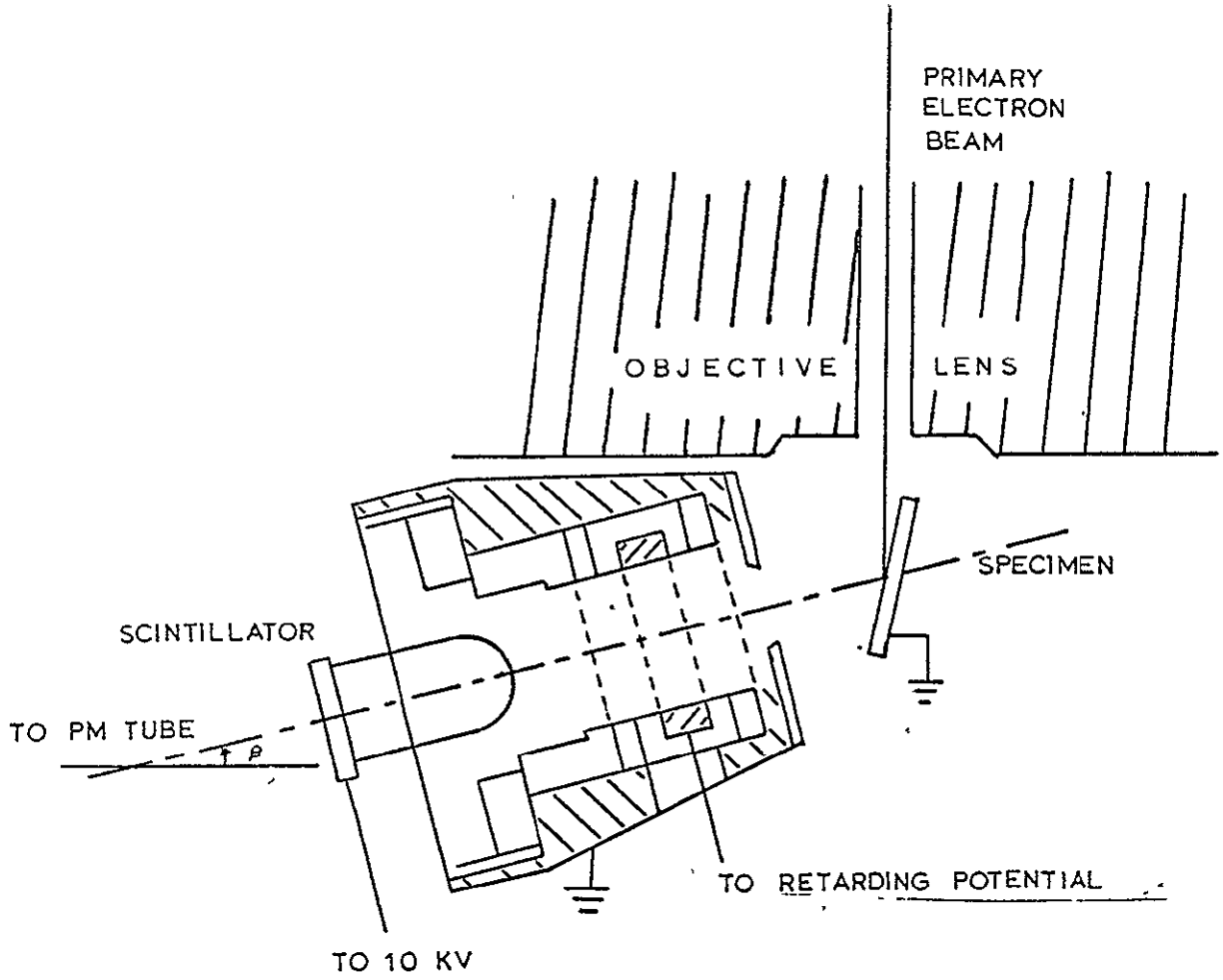

FIGURE 3

SCHEMATIC OF THE AUGER DETECTOR. THE ANGLE θ CAN ASSUME A VALUE OF EITHER 0° OR 12°

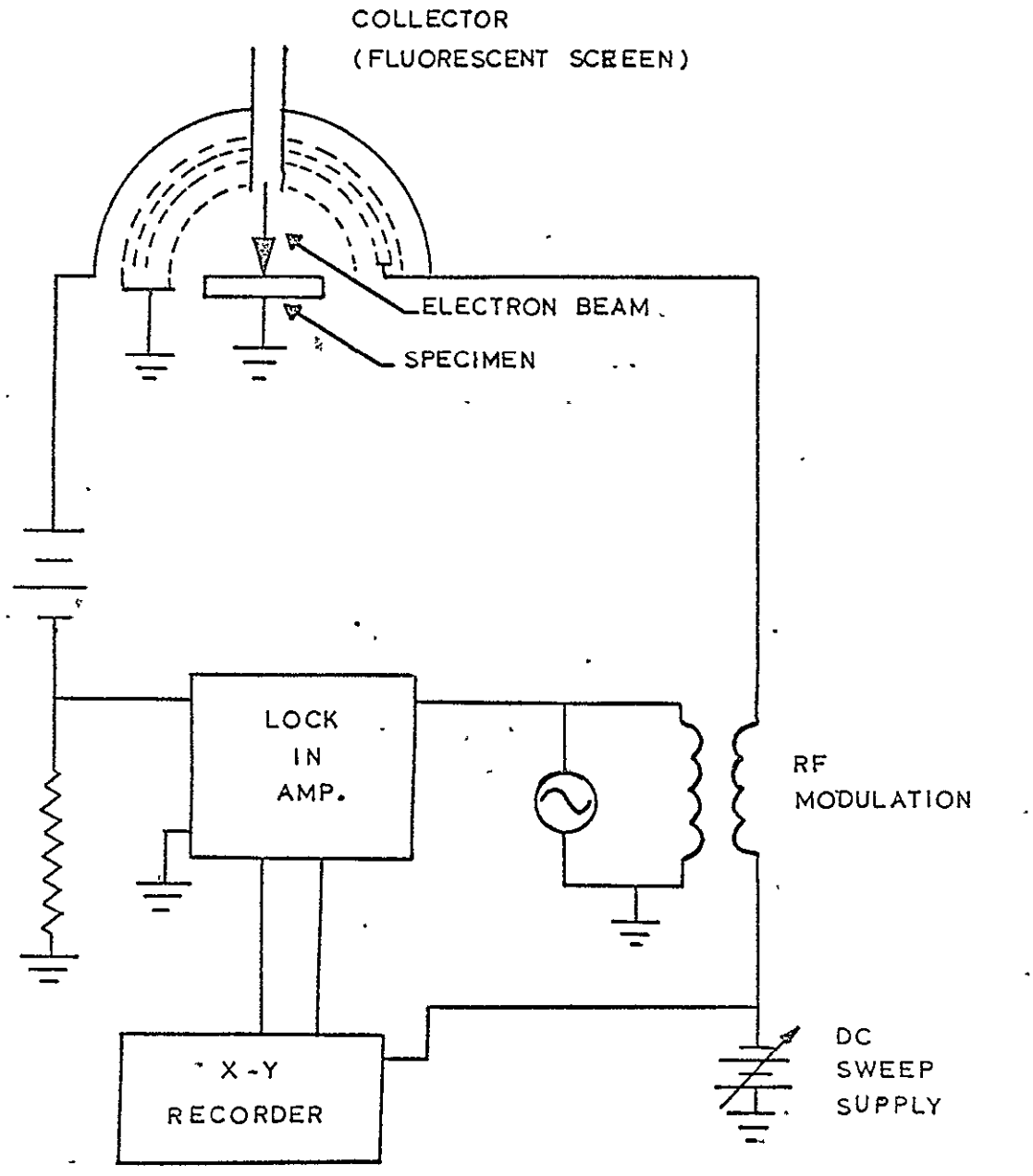

FIGURE 4.

A LEED TYPE RETARDING FIELD ANALYZER

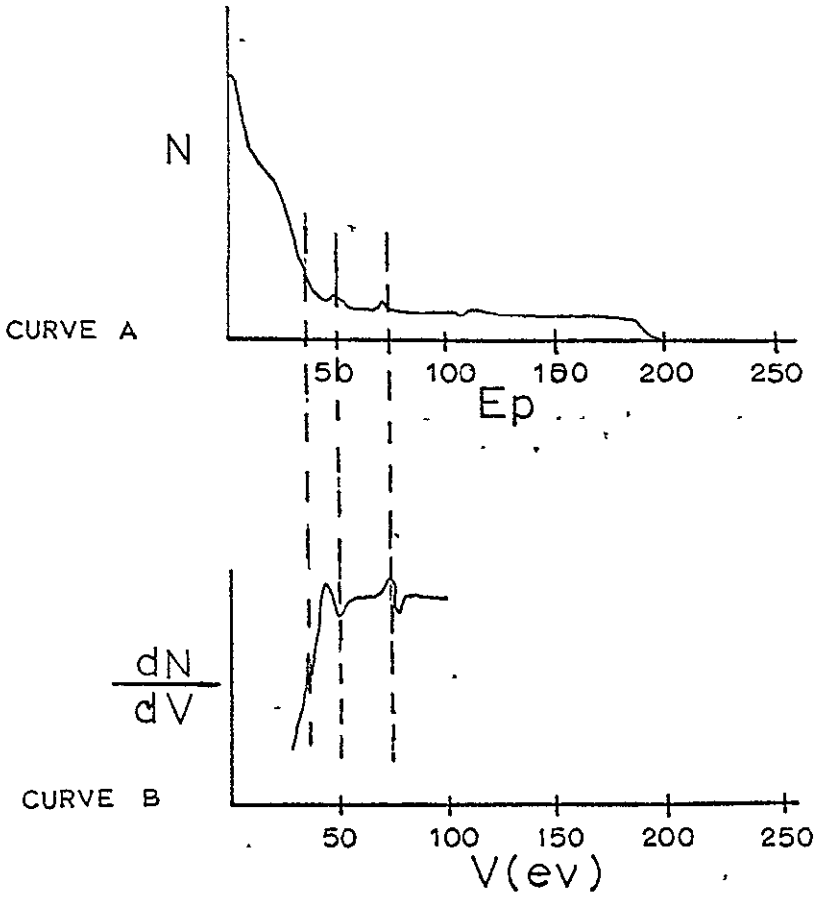

FIGURE 5

AN EXAMPLE OF THE ENCHANCEMENT OF AUGER PEAKS WHEN ENERGY DISTRIBUTION (CURVE A) IS DIFFERENTIATED (CURVE B) IN THE RETARDING FIELD TECHNIQUE

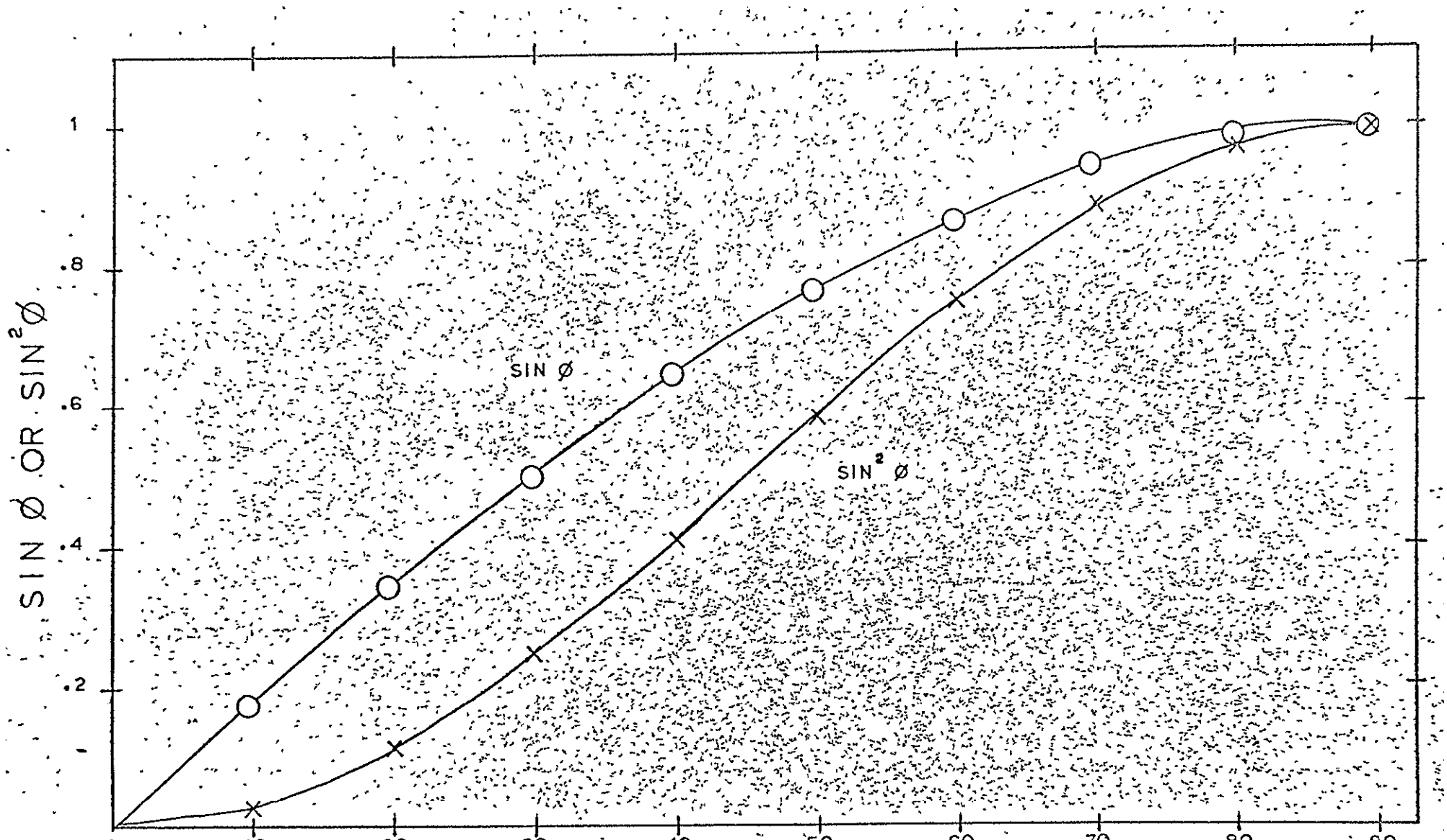

FIGURE 6

A PLOT OF THE RESOLUTION VS APERTURE OPENING FOR ϕ = 0° TO 90°

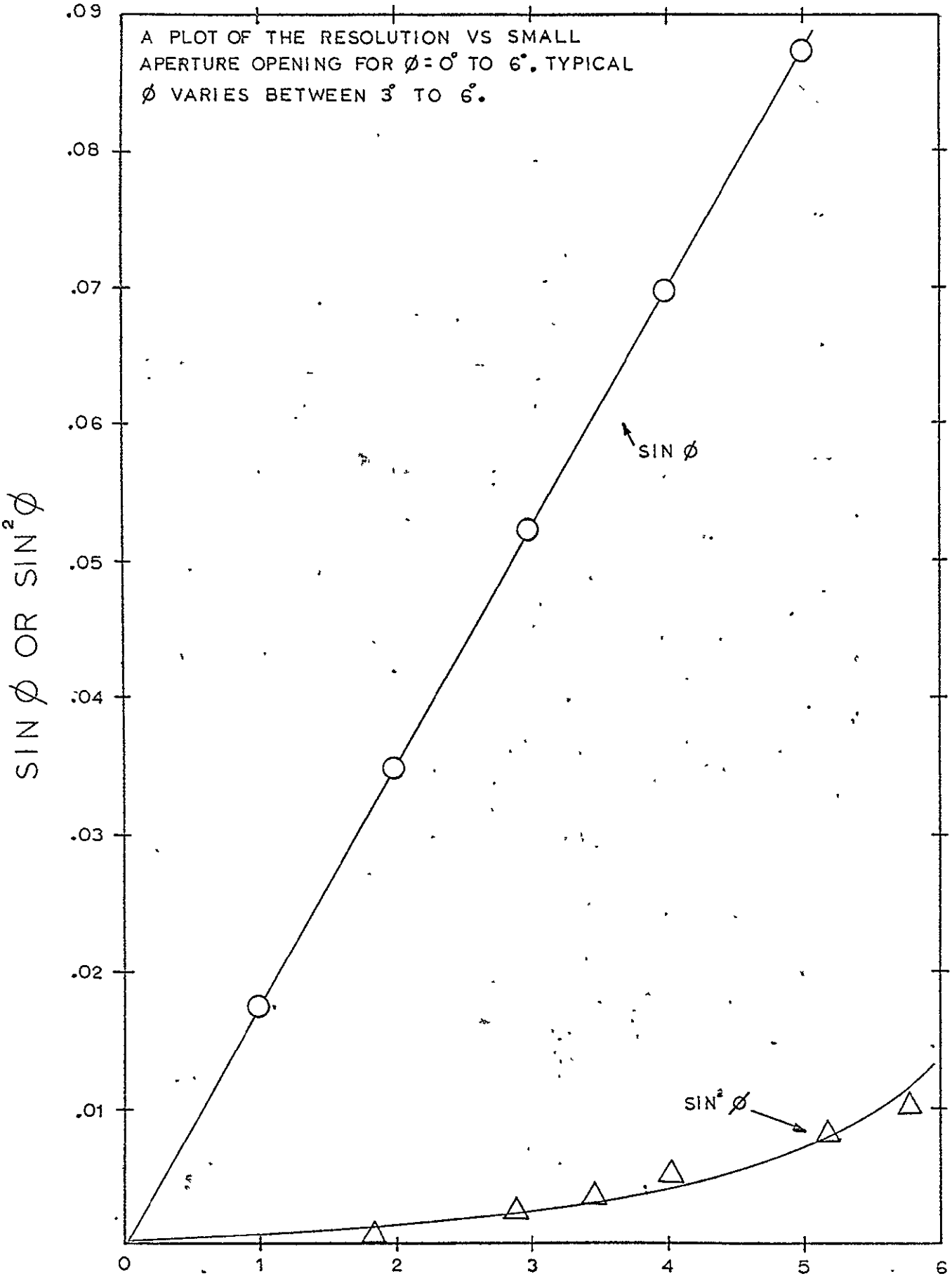
A PLOT OF THE RESOLUTION VS SMALL APERTURE OPENING FOR Ø = 0° TO 6°. TYPICAL Ø VARIES BETWEEN 3° TO 6°.
SIN Ø OR SIN² Ø
.09
.08
.07
.06
.05
.04
.03
.02
.01
SIN Ø
SIN² Ø
0
1
2
3
4
5
6
APERTURE IN DEGREES

FIGURE 7

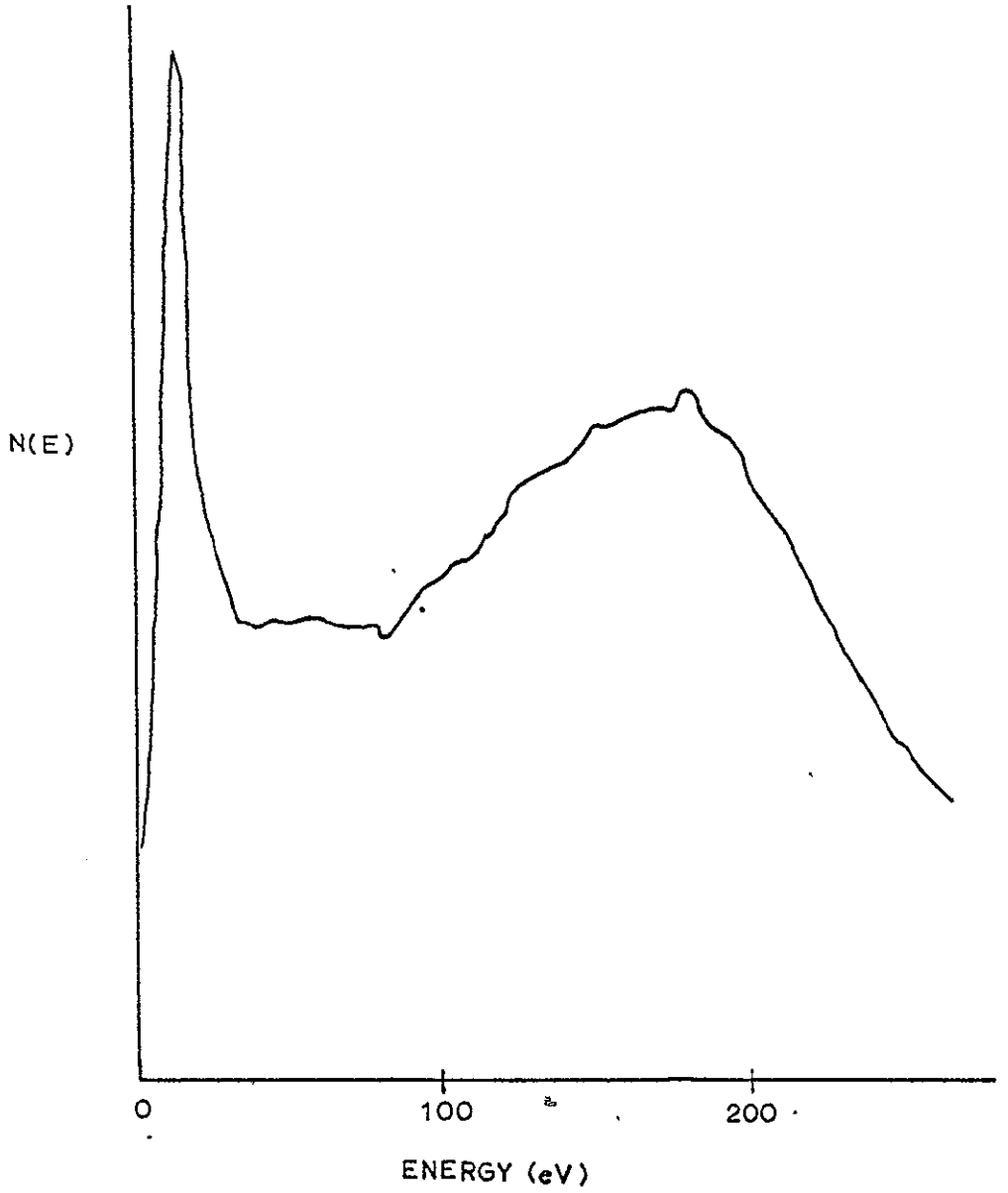

FIGURE 8A

A GOLD SPECTRUM WHEN THE DETECTOR IS 2 mm FROM THE SAMPLE. THE 70 eV PEAKS ARE NOT RESOLVED.

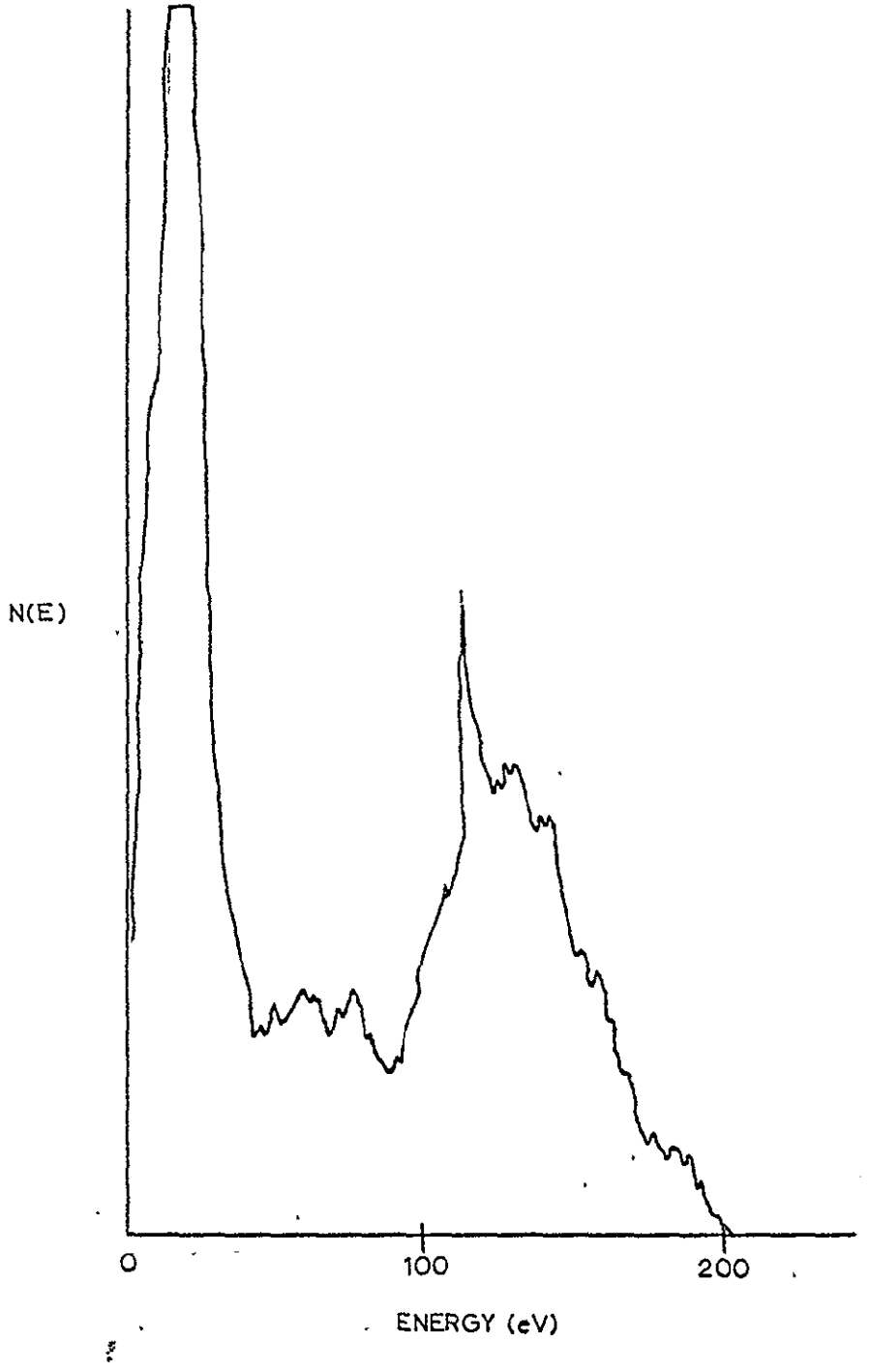

FIGURE 8B

THE SAME SPECTRUM WHEN THE DETECTOR IS ABOUT 2 cm AWAY FROM THE SAMPLE. THE 55, 66, AND 80 eV PEAKS ARE RESOLVED

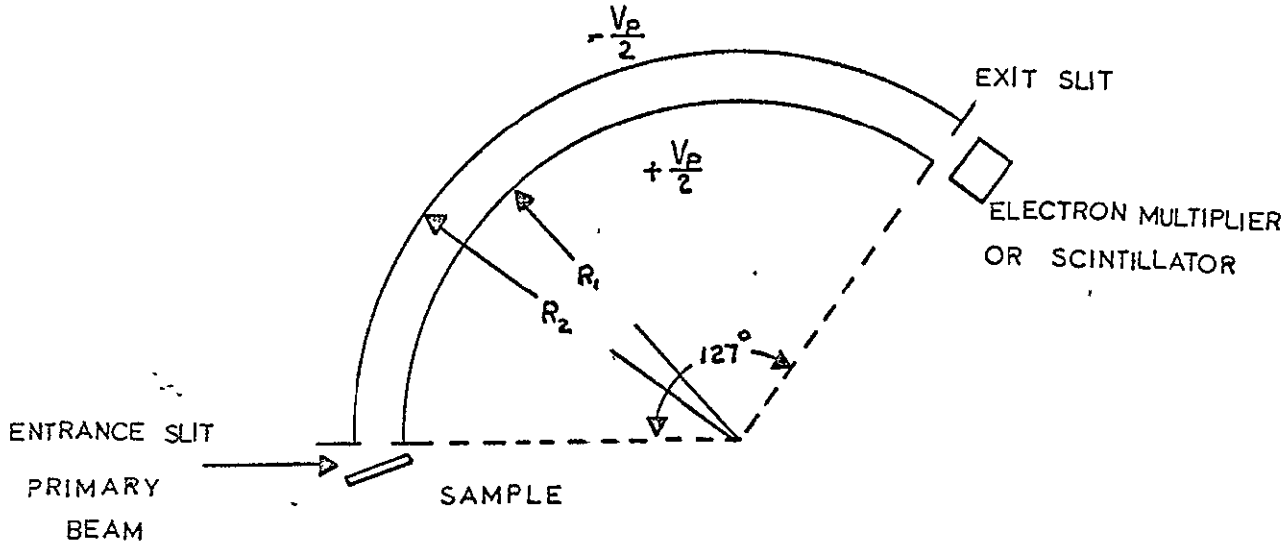

FIGURE 9
SCHEMATIC OF THE
127° SECTOR ANALYZER

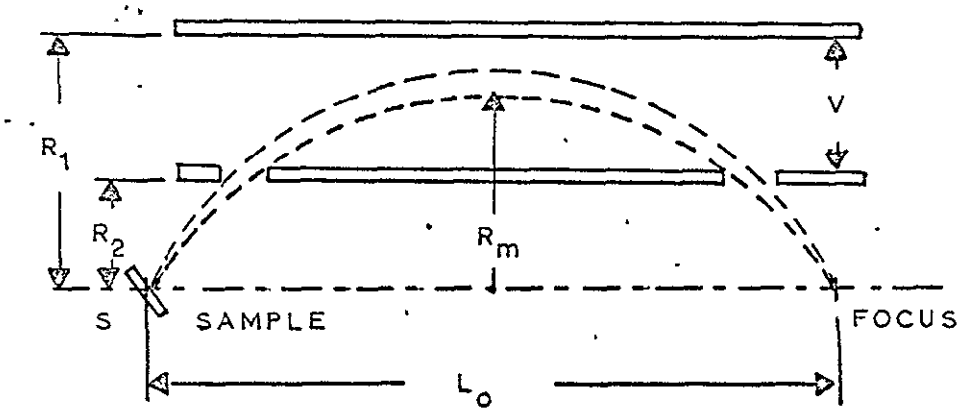

FIGURE 10

A SCHEMATIC DIAGRAM OF THE 180° CYLINDRICAL MIRROR ANALYZER

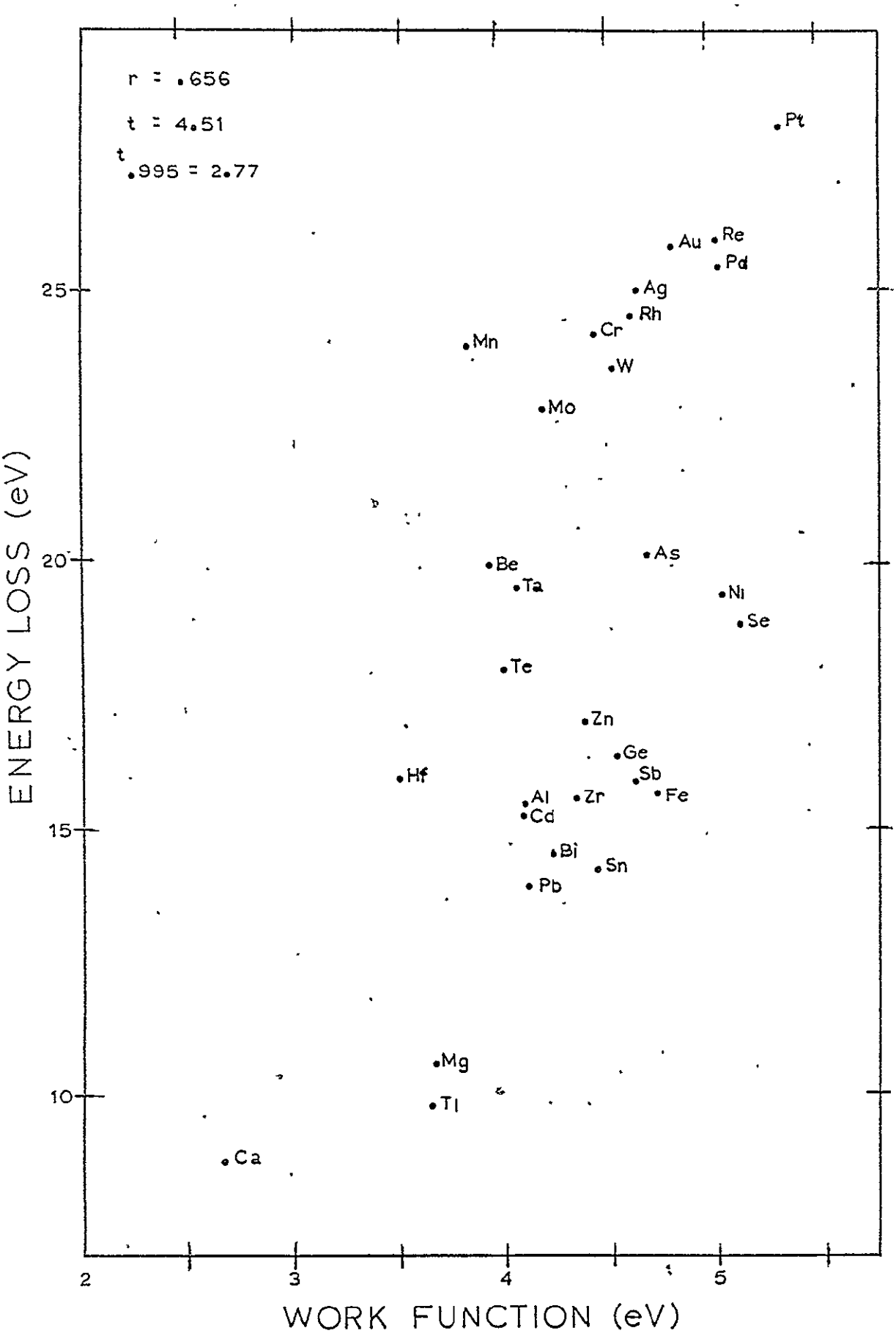

FIGURE 11

CORRELATION OF ENERGY LOSS AND WORK FUNCTION

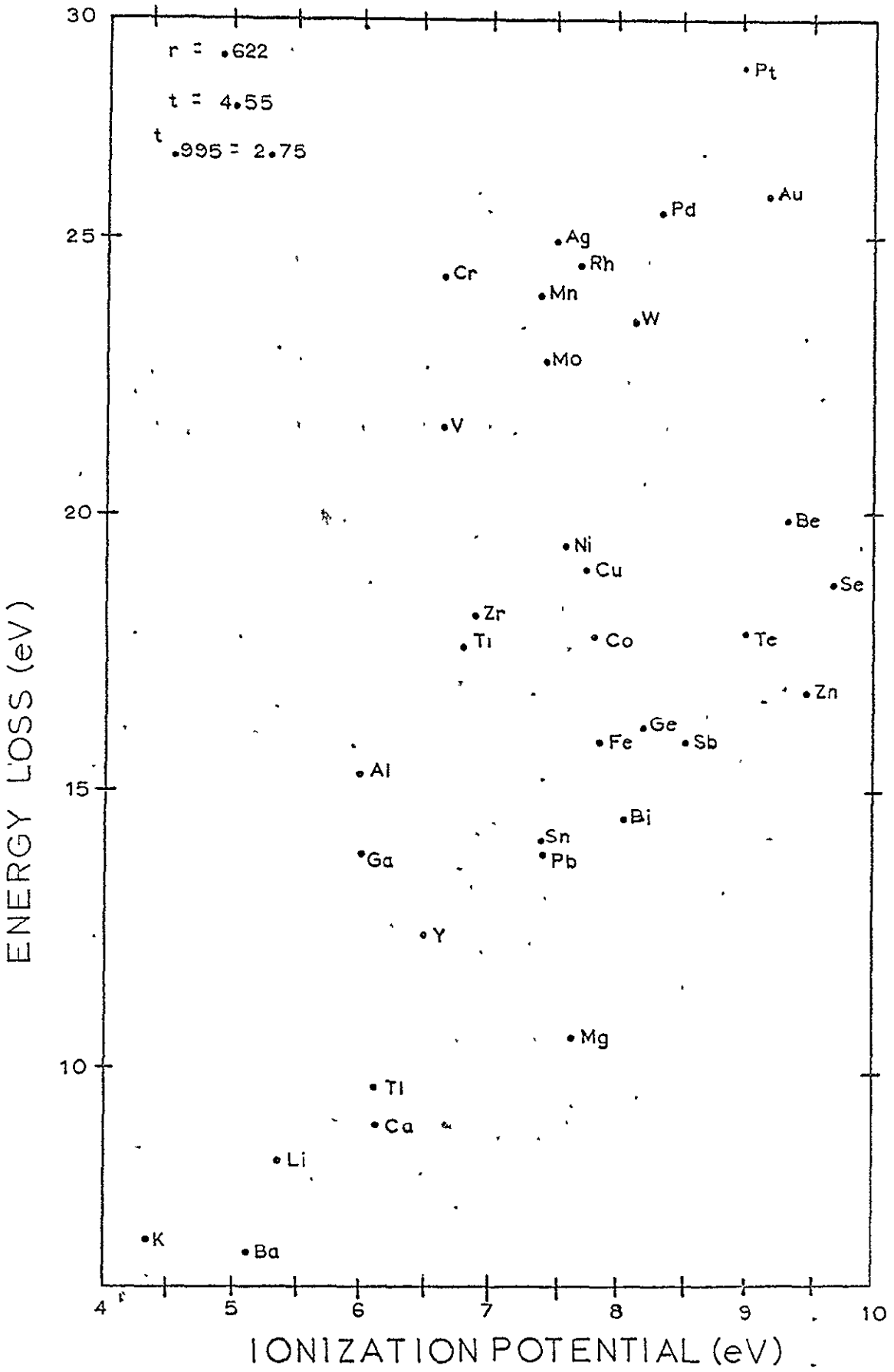

FIGURE 12

CORRELATION OF ENERGY LOSS AND IONIZATION POTENTIAL

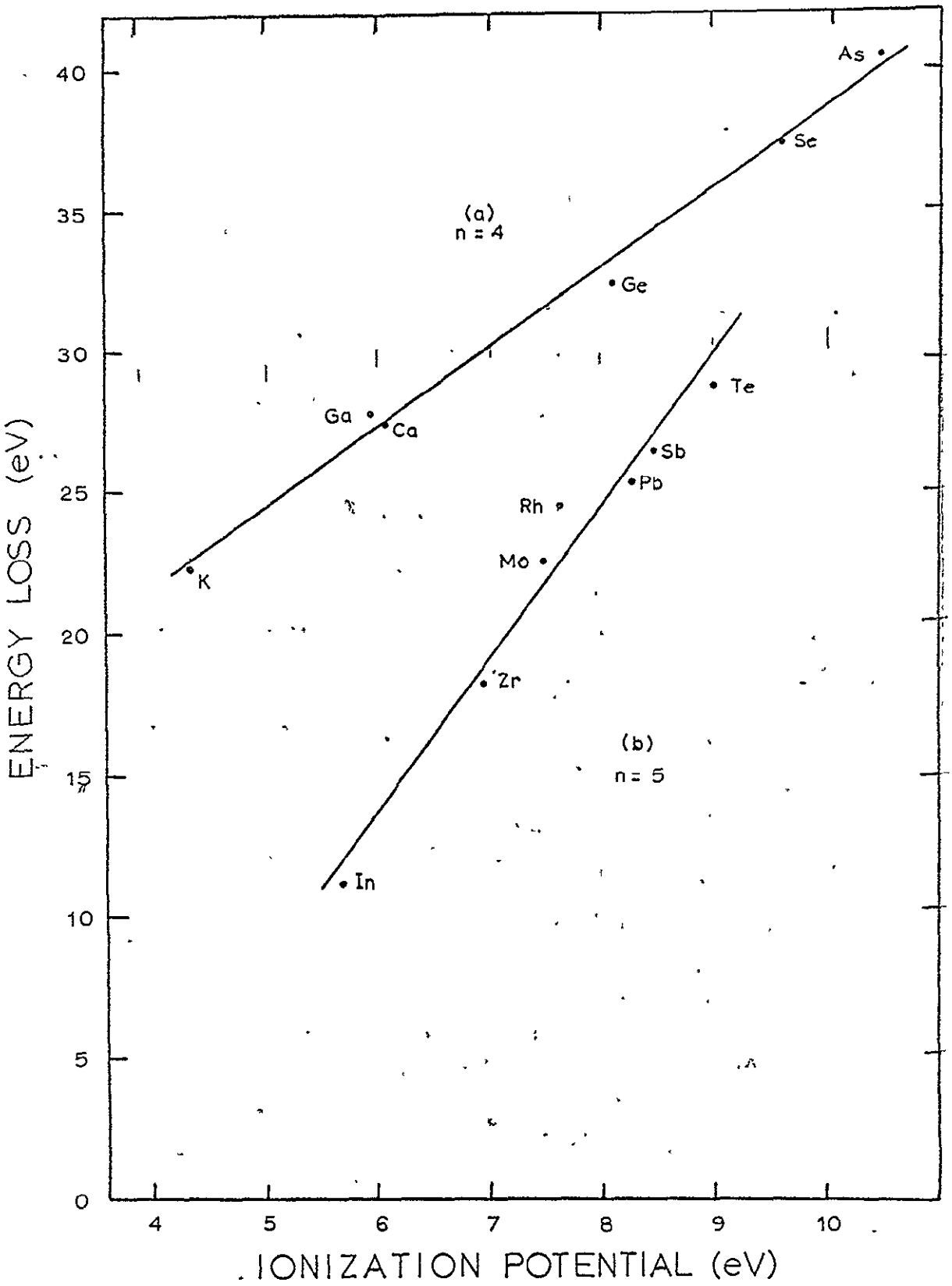

FIGURE 13

ENERGY LOSS TRENDS

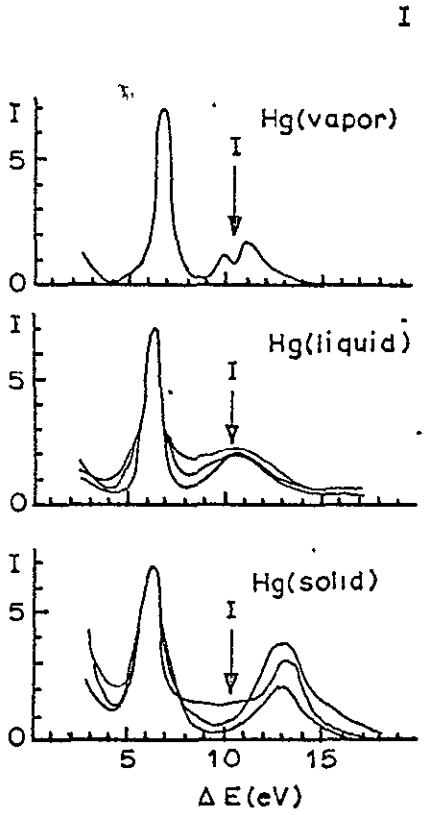

CHARACTERISTIC ENERGY LOSSES IN MERCURY SOLID, LIQUID, AND VAPOR

FIG 14

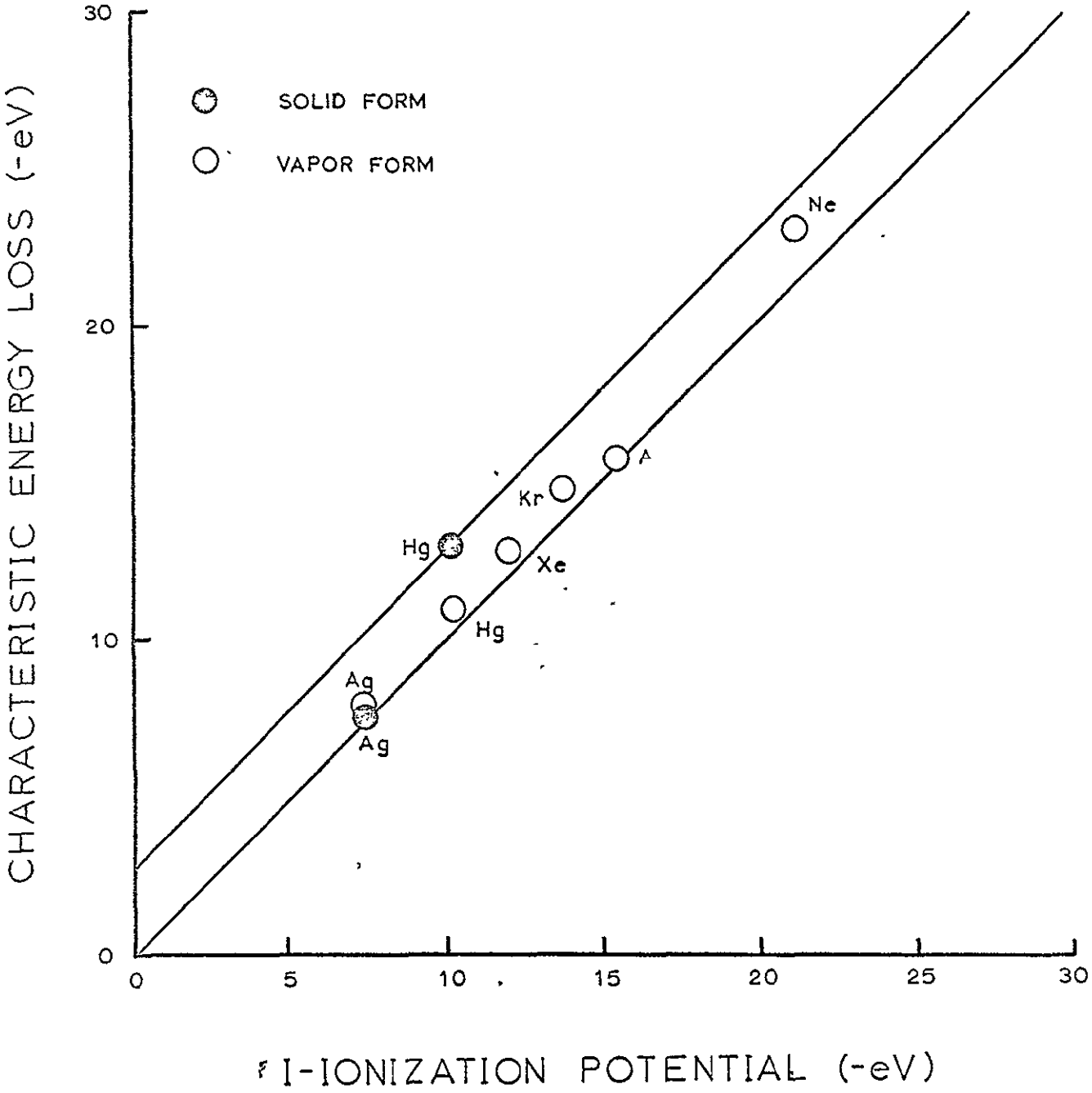
CHARACTERISTIC ENERGY LOSS (-eV)
30
20
10
0
SOLID FORM
VAPOR FORM
Ne
A
Kr
Xe
Hg
Hg
Ag
Ag
0
5
10
15
20
25
30
I-IONIZATION POTENTIAL (-eV)

FIG 15

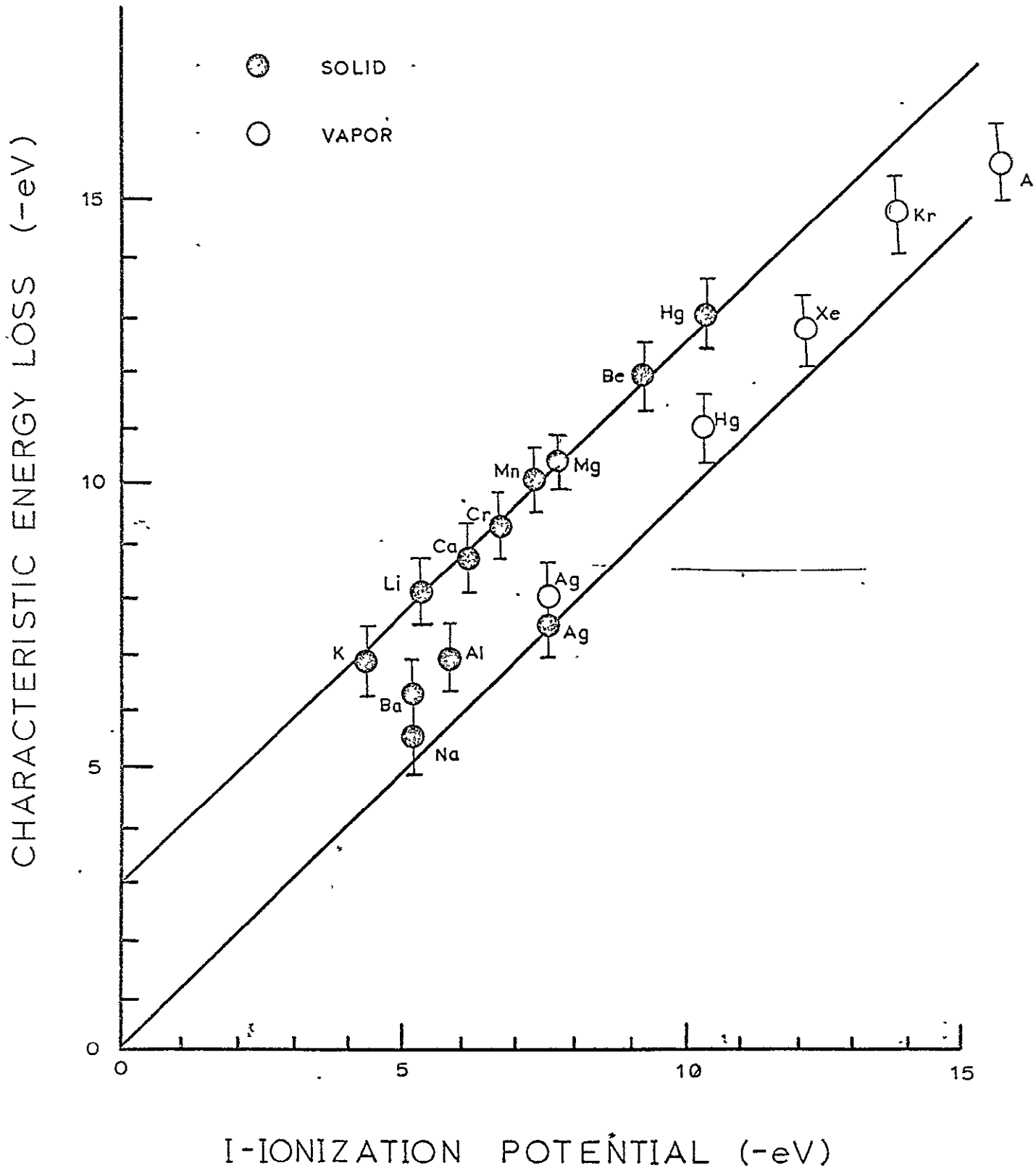
SOLID
VAPOR
CHARACTERISTIC ENERGY LOSS (-eV)
I-IONIZATION POTENTIAL (-eV)
0
5
10
15
A
Kr
Xe
Hg
Hg
Be
Mg
Mn
Cr
Ca
Li
Ag
Ag
K
Al
Ba
Na

FIG 16

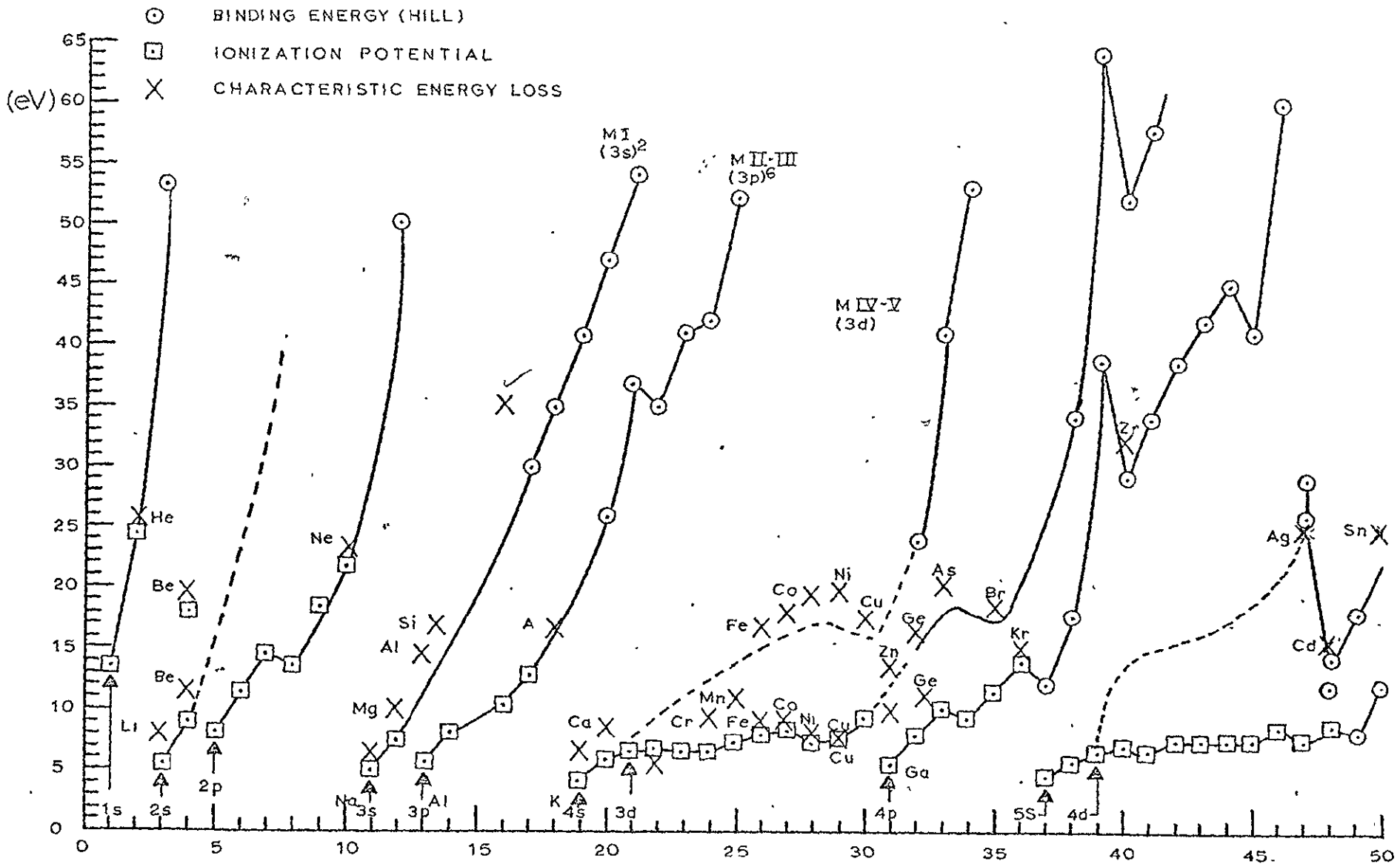

ATOMIC NUMBER (Z)

FIG 17

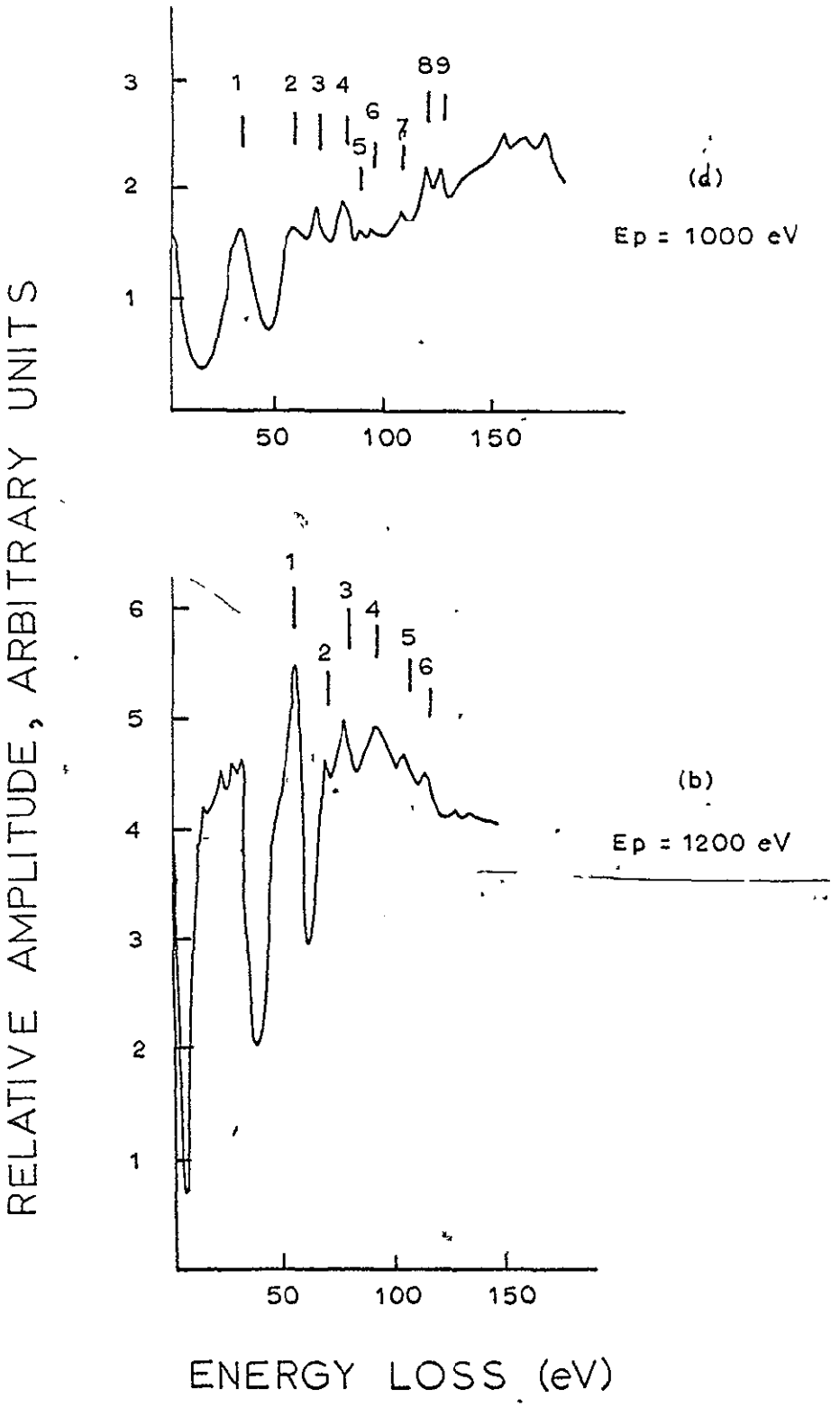

FIGURE 18

CHARACTERISTIC ENERGY LOSS IN ALUMINUM

TABLE 1

AUGER'S RESULTS ON THE FLUORESCENCE YIELD

ELEMENT	Wk	WL
A - 18	0.07	
Kr - 36	0.51	0.1
Xe - 54	0.71	0.25

TABLE 2

FLUORESCENCE YIELDS IN THE K SERIES

ELEMENT	AUGER	BALDER STON	HARMS	MARTIN	COMPTON	LOCHER	HASS
8 O						0.082	
10 Ne						0.083	
12 Mg							0.013
14 Si							0.038
16 S							0.083
17 Cl							0.108
18 A	0.07					0.149	
20 Ca							0.150
24 Cr							0.263
26 Fe		0.33	0.28	0.29			
28 Ni		0.39		0.35	0.37		
29 Cu		0.44	0.38	0.40			
30 Zn		0.50	0.40	0.46			
34 Se			0.52	0.59	0.55		
35 Br				0.59	0.56		
36 Kr	0.51						
38 Sr			0.62				
42 Mo		0.83	0.73		0.68		
47 Ag		0.75					
53 I				0.75			
54 Xe	0.70						

TABLE 3

CHARACTERISTIC ENERGY LOSSES IN TRANSITION ELEMENTS
(Lynch and Swan)

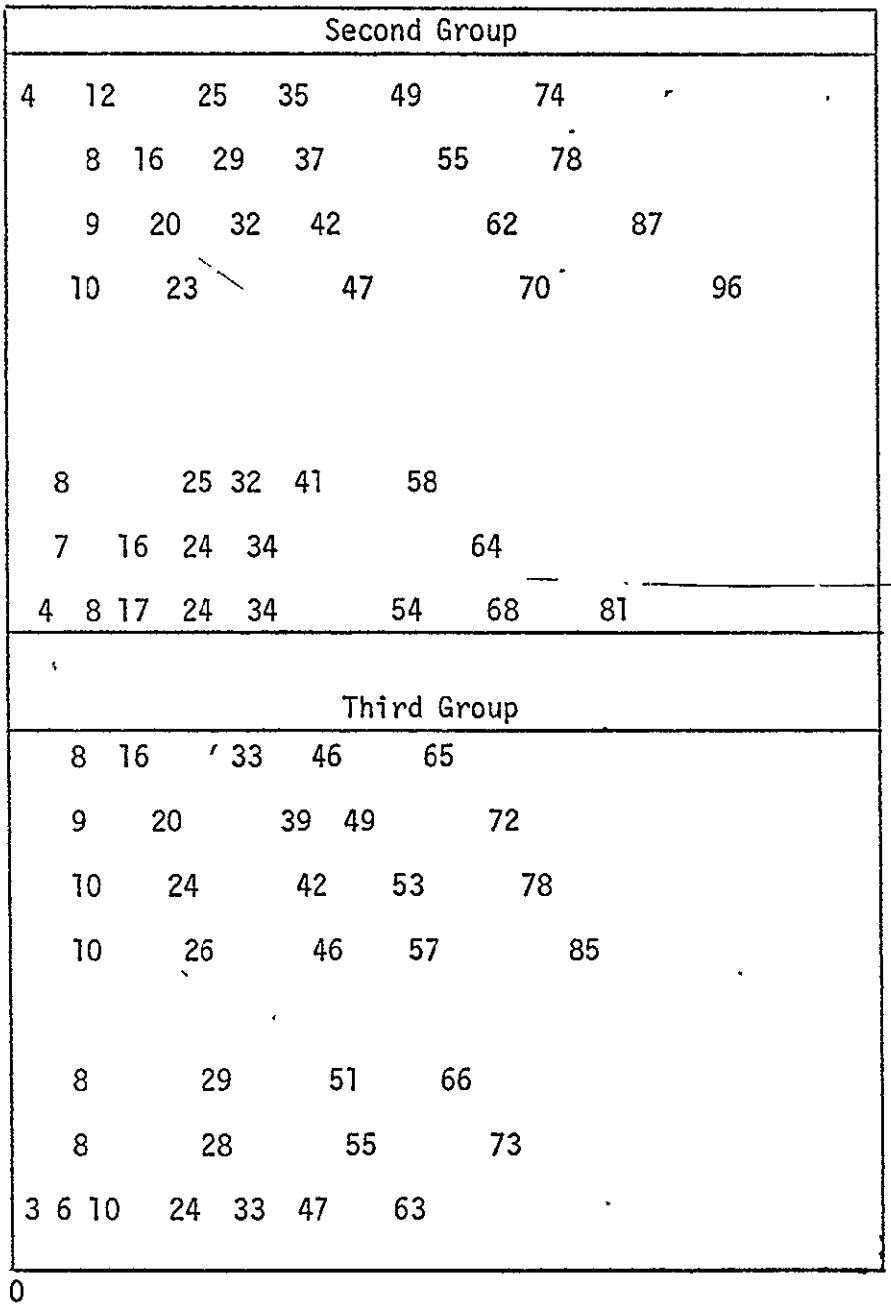

TABLE .4

CHARACTERISTIC ENERGY LOSSES IN ALUMINUM

AS MARKED IN FIGURE 3

(a) Ep = 1000 eV		(b) Ep = 1200 eV	
PEAK NUMBER	ENERGY LOSS (eV)	PEAK NUMBER	ENERGY LOSS (eV)
1	34		
2	63	1	61
3	73	2	72
4	85	3	85
5	92		
6	97	4	98
7	112	5	111
8	124	6	122
9	132		

TABLE 5

PRESENT WORK COMPARED TO PREVIOUS WORK AND X-RAY DATA

ELECTRON ENERGY LOSS (eV)		X-RAY ABSORPTION (eV)
PRESENT WORK	SWANSON AND POWELL	
	15	
34	30	
	45	
63	60	
73	72.5	72.7
	76.8	76
85		84
97	96.8	96
112	111.7	112
124	124.7	125

References

1. J.J. Lander, Phys. Rev., 91:1382, (1953).
2. H. Hafner, Rev. Sci. Instrum., 39:33, (1968).
3. R.E. Weber and W.T. Beria, J. Appl. Phys., 38:4355, (1967).
4. J.J. Lander, Ibid.
5. L.N. Tharp and E.J. Scheibner, J. Appl. Phys., 38:3320, (1967).
6. L.A. Harris, J.Appl. Phys., 39:1428, (1968).
7. E.H. Bishop and J.C. Riviere, J. Appl. Phys., 40:1740, (1969).
8. N.C. MacDonald, H.L. Marcus and P.W. Palmberg, Scanning Electron Microscopy/70, Chicago, 1970, p. 25.
9. R. Whiddington, Proc. Roy. Soc. A., 86:360 (1912)
10. Compton and Allison, X-Ray in Theory and Experiment, New York, 1935.
11. L.N. Tharp and E.J. Scheibner, Ibid.
12. R.E. Weber and W.T. Peria, Ibid.
13. N.J. Taylor, Rev. Sci. Instrum., 40:792, (1969).
14. E.H. Bishop and J.C. Riviere, Ibid.
15. N.J. Taylor, Ibid.
16. Hughes and Rojansky, Phys. Rev., 34:284, (1929).
17. L.A. Harris, J.Appl. Phys., 39:1419, (1968).
18. E. Blauth, Z. Physik., 147:228, (1951).
19. V. Zashkuara, Soviet Phys.-Tech. Phys., 11:96, (1966).
20. H.Z. San-el, Rev. Sci. Instrum., 28:1210, (1967).
21. P.N. Plamberg, Appl. Phys. Letters, 15:276 (1969).
22. E.H. Bishop and J.C. Riviere, Ibid.
23. L. Martin, L.B. Leder and H. Mendlowitz, Advances in Electronics and Electron Physics, New York, 1955, p. 183.
24. J.A. Becker, Phys.Rev., 23:664, (1924).

25. D. Brown and R.Whiddington., Proc. Leeds Phil. Lit.Soc., 1:162, (1927).

26. E. Rudberg, Phys. Rev., 50:138, (1936)-

27. G. Ruthemann, Ann. Physik., 26:113, (1948).

28. E. Rudberg and J.C. Slater, Phys. Rev., 50:150 (1936).

29. V.W. Richardson, Proc. Phys. Soc., London, 1930, p. 63.

30. Y. Cauchois, Acta Cryst., 5:351, (1952).

31. L.B. Leder, Phys. Rev., 103:1721, (1956).

32. D. Klemperer and J.P.G. Shepherd, Advances in Sci., 12:364, (1963).

33. A.J. Ivietskin, Sov. Phys.-Tech. Phys., 3:2038, (1958).

34. E.J. Sternglass, Nature, 178:1387, (1956).

35. H. Raether, Springer Tracts in Modern Physics, Berlin-Heidelberg, 1965, P. 154.

36. N. Swanson and C.J. Powell, Phys. Rev., 167:592, (1967).

37. H. Watanabe, J. of Appl. Phys.-Japan., 3:804,(1964).

38. N. Swanson and C.J. Powell, Ibid.

39. V.V. Rumyantsev, Sov. Phys.-Solid State, 9:1860 (1968).

40. J. Thirwell, J. of Phys. Chem. (Proc. of Phys. Soc.), 1, Ser 2:979, (1968).

41. R.E. Burge and D.I. Misell, Philosophy Man., 18:261, (1968).

42. G.C. Hale and J.B. Hasted, Nature, 217:945, (1949).

43. M.J. Lynch and J.B. Swan, Australian J. of Phys., 21:811, (1968).

44. O. Klemperer and J.P.G. Shepherd, Ibid.

45. M.J. Lynch and J.B. Swan, Ibid.

46. L. Siegbahn, Handbook der Physiks, Berlin, 1968.

47. C.J. Powell, J.L. Robins and J.B. Swan, Phys. Rev., 110:657, (1958).

48. A. Huen, Master's Thesis, University of Pittsburgh, 1970.

49. G.A. Harrower, Rev. of Sci. Instrum., 26:850 (1955).

50. N. Swanson and C.J. Powell, Ibid.

51. H. Wanatabe, Ibid.